M 2022

U.PORTO
FEUP FACULDADE DE ENGENHARIA
UNIVERSIDADE DO PORTO

DEVELOPMENT OF ENGINEERED CATALYSTS FOR THE LOW TEMPERATURE METHANE DECOMPOSITION

RICARDO ANDRÉS MARQUES COELHO
MASTER THESIS IN CHEMICAL ENGINEERING
PRESENTED TO THE FACULTY OF ENGINEERING
OF THE UNIVERSITY OF PORTO

Master in Chemical Engineering

Development of engineered catalysts for the low temperature methane decomposition

Master dissertation

of

Ricardo Andrés Marques Coelho

Developed within the course of dissertation

held in

Pixel Voltaic Lda.

PIXEL VOLTAIC

Supervisor at FEUP: **Dr. Paula Dias**

Joint supervisor at FEUP: **Prof. Adélio Mendes**

Coordinator at Pixel Voltaic: **Eng. Francisco Neto**

U.PORTO
FEUP FACULDADE DE ENGENHARIA UNIVERSIDADE DO PORTO

DEPARTAMENTO DE ENGENHARIA QUÍMICA

October 2022

Acknowledgment

I want to start by thanking Pixel Voltaic for given me the opportunity to develop my master thesis on such an interesting subject, for all the knowledge transmitted, and for the job experience. I have to say that I grew so much in the last months, and I am glad for the amazing experience that I had. This internship has given me the certainty of the direction and contribution I intend to make in the future as a chemical engineer.

I would like to give a special thanks to the supervisor at FEUP, Dr. Paula Dias and my co-supervisor Prof. Adélio Mendes for the guidance and much needed corrections, as well as to Tiago Lagarteira for the availability to meet with me, help me structuring my dissertation and answer all my questions whenever necessary. Also, to PhD researchers Vítor Pereira and Luís Alves, for teaching me all the laboratory procedures, theoretical backgrounds, the everyday help, and advice, without whom I would not have ever been able to complete this work. In addition, thanks to my supervisor at Pixel Voltaic, Eng. Francisco Neto and to all involved in the company, the effort to make me feel integrated. To the entire LEPABE – Laboratory for Process Engineering, Environment, Biotechnology and Energy – team. It has been a pleasure to work with such a nice and diverse team that always made me feel welcomed.

To all my friends that supported me throughout this semester. Thanks for the great times, crucial for maintaining my mental health. Specially to my fellow musketeers Hugo Cruz and Luís Porto for the everyday company. Finally, I am beyond grateful to my mother, my father, my sister, and all my closest family, for all the love, the endless support, and for making it possible for me to study and complete my goals throughout all these years.

Abstract

The world needs a disruptive technology to quickly decarbonize the energy sector. The EU alone aims at reducing 55 % of the greenhouse gas emissions of by 2030 and reaching neutrality by 2050. The success of this technology critically depends on its social acceptance, fast implementation, sustainability and low-cost. Hydrogen has gained momentum as an energy vector, and it is considered a key element for the current energy transition scenario. Currently, steam methane reforming is responsible for *ca.* 95 % of hydrogen production, but it releases large amounts of CO_2; green hydrogen produced by electrolysis is 3-4 times more expensive. Methane decomposition has a unique potential to accelerate the transition from the current carbon economy towards the foreseen hydrogen economy. Natural gas or biomethane can be used for running the methane decomposition reaction to produce clean hydrogen and solid carbon; if biomethane is used, the process is then CO_2 negative.

Catalytic methane decomposition (CMD) avoids the excessive thermal decomposition requirements of the non-catalytic reaction, reducing the operation temperature from > 1000 °C to 450-850 °C. CMD systems are not yet widespread due to catalyst deactivation, caused by solid carbon formation. This phenomenon can be surpassed through the periodic regeneration of the catalyst and the use of improved membrane reactor design to increase the lifetime of the catalyst. The catalytic membrane has also a critical role on the hydrogen produced and type of carbon growth. Metal catalysts are the most used materials for the CMD reaction, being nickel-based catalysts the most promising ones due to their high stability and catalytic activity.

In the present work, successive ionic layer adsorption and reaction (SILAR) was used to deposit thin and conformal films of NiO on top of alumina ceramic substrates; to the best knowledge of the authors, this is the first time that this technique is used for these applications. The SILAR deposition conditions were varied and their influence on the film morphology and catalytic activity was studied running the reactor at 550 ºC over 1 h. The high-performing catalytic membrane was prepared using $Ni(NO_3)_2{\cdot}6H_2O$ as the cationic precursor and H_2O_2 1 % (v/v) as the anionic precursor; a peak catalytic activity of *ca.* 45.6 $g_{H2}\ g_{cat}^{-1}\ h^{-1}$ was obtained, which clearly demonstrates the ideal crystallography of the obtained structures to promote methane decomposition. However, the use of H_2O_2 impairs a poor dispersion of the active sites that leads to very short catalytic stability. Alternatively, NaOH solution was used, and the influence of its concentration was studied, as well as the effect of using rinse steps. The best performing membrane, both in terms of activity and stability, was prepared using 0.1 M NaOH solution, 10 cycles with rinse steps. An unprecedented average activity of *ca.* 23.3 $g_{H2}\ g_{cat}^{-1}\ h^{-1}$ was obtained, which is 4 to 5 times higher than the best value reported in the literature (test ran at 650 ºC).

Keywords: Energy decarbonization, hydrogen, catalytic methane decomposition, catalytic membrane, Nicked-based catalysts, SILAR

Resumo

O mundo necessita de uma tecnologia capaz de prontamente descarbonizar o setor energético. A União Europeia tem como objetivo reduzir 55 % das emissões de gases de efeito de estufa até 2030 e tornar-se neutra carbonicamente até 2050. O sucesso desta tecnologia depende bastante da sua aprovação social, rápida implementação, sustentabilidade e reduzido custo. O hidrogénio tem ganho impulso como vetor energético e é considerado um elemento-chave para o atual cenário de transição energética. Atualmente, a reformação do metano é responsável por cerca de 95 % do hidrogénio produzido, mas liberta grandes quantidades de CO_2; o hidrogénio verde produzido através da eletrólise é, por sua vez, 3 a 4 vezes mais caro. Por sua vez, a decomposição de metano surge com uma tecnologia com elevado potencial para acelerar a transição energética e, consequentemente, produção de hidrogénio limpo e barato. O gás natural ou o bio metano podem ser utilizados para promover a reação da decomposição de metano e produzir hidrogénio e carbono no estado sólido; se for utilizado bio metano, o processo passa a ter emissões carbónicas negativas.

A decomposição de metano catalítica (CMD) permite reduzir os elevados consumos térmicos da reação não-catalítica (temperaturas de operação >1000 °C) e operar a temperaturas entre 450 – 850 °C. A desativação do catalisador causada pela formação de carbono sólido é o principal problema dos sistemas de CMD, no entanto, este fenómeno pode ser reduzido através de um período de regeneração do catalisador e otimização do desenho de reator de forma a aumentar o tempo de vida do catalisador. A membrana catalítica tem um papel fundamental na produção de hidrogénio e no tipo de carbono produzido. Os catalisadores metálicos são os mais usuais para a reação de CMD, sendo os à base de níquel mais promissores devido à sua alta estabilidade e atividade catalítica.

Neste trabalho, a técnica de adsorção e reação sucessiva de camadas iónicas, do inglês *successive ionic layer adsorption and reaction* (SILAR), foi utilizada para depositar filmes finos de NiO na superfície de substratos cerâmicos de alumina; do conhecimento dos autores, é a primeira vez que esta técnica é utilizada neste tipo de sistemas. As condições da deposição por SILAR foram variadas e a sua influência foi estudada, sendo o reator operado a 550 °C durante 1 h. A membrana catalítica preparada, usando $Ni(NO_3)_2{\cdot}6H_2O$ como o precursor catiónico e H_2O_2 com 1 % (v/v) como precursor aniónico, obteve altos valores de atividade catalítica (atividade máxima de 45.6 $g_{H2}\ g_{cat}^{-1}\ h^{-1}$), o que claramente demonstra que as estruturas cristalinas obtidas têm a estrutura ideal para a decomposição de metano. Contudo, a utilização de H_2O_2 provoca uma baixa dispersão das áreas ativas que leva a uma reduzida estabilidade catalítica. Em alternativa, estudou-se o uso de uma solução catiónica de NaOH e a existência de uma fase de lavagem da membrana foi estudada. A membrana com o melhor desempenho, tanto em termos de atividade como de estabilidade, foi preparada utilizando uma solução de NaOH com 0.1 M,

10 ciclos de deposição e imersão em soluções de lavagem. Obteve-se uma atividade média de 23.3 g_{H2} g_{cat}^{-1} h^{-1}, sendo 4 a 5 vezes superior ao maior valor relatado na literatura (neste caso, operando o reator a 650 °C).

Palavras-chave: Descarbonização de energia, hidrogénio, decomposição de metano catalítica, membrana catalítica, catalisadores à base de níquel, SILAR.

Declaration

I hereby declare, under word of honour, that this work is original and that all non-original contributions is indicated and due reference is given to the author and source

Ricardo Andrés Marques Coelho

(Ricardo Andrés Marques Coelho)

26 September 2022

Index

List of Figures

List of Tables

Notation and Glossary

a	Activity	$g_{H2}\ g_{cat}^{-1}\ h^{-1}$
X_{CH4}	Conversion	
Q	Flow	$m^3\ s^{-1}$
m	Mass	Kg
M	Molar Mass	$g\ mol^{-1}$
n	Number of moles of a substance	mol
d_m	Particle Diameter	m
T	Temperature	K
t	Time	s

List of Acronyms

ALD	Atomic Layer Deposition
BSD	Backscattered Electron Display
CBD	Chemical Bath Deposition
CDM	Catalytic Decomposition of Methane
CNT	Carbon Nanotubes
EU	European Union
FBR	Fluidized Bed Reactor
GHG	Green House Gases
HER	Hydrogen Evolution Reaction
ICP-MS	Inductively Coupled Plasma - Mass Spectrometry
LTMD	Low Temperature Methane Decomposition
MD	Methane Decomposition
MMR	Molten-Metal Reactor
MR	Membrane Reactor
OER	Oxygen Evolution Reaction
PEC	Photoelectrochemical
PEM	Proton Exchange Membrane
PR	Plasma Reactor
SED	Secondary Electron Display
SEM	Scanning Electron Microscope
SILAR	Successive Ionic Layer Adsorption and Reaction
SRM	Steam Reforming of Methane
TRL	Technology Readiness Level

1 Introduction

1.1 Framing and presentation of the work

For more than two decades, the growing threat of global warming and climate change has been a serious worldwide concern. The Intergovernmental Panel on Climate Change stated, for the first time in 1995, “that there is a discernible human influence on global climate” [1]. After the Industrial Revolution, human society has witnessed an unprecedented technological development, with fossil fuels in the spotlight of energy sources. The energy demand never stopped growing as the world population started to increase exponentially. Emissions of greenhouse gases (GHG) have continuously increased due to the consumption of fossil fuels, leading to an accelerated global warming phenomenon with severe consequences to the climate stability of planet Earth. Figure 1 demonstrates the direct influence of the rise of the CO_2 levels (blue area), on the mean temperature on the surface of the Earth since the 18th century (black line). At present, there is a global consensus to implement drastic changes in the way energy is provided, stored, and consumed, forcing an extensive reduction of GHG emissions aiming at keeping global warming below 2 °C relatively to the pre-industrial times [2].

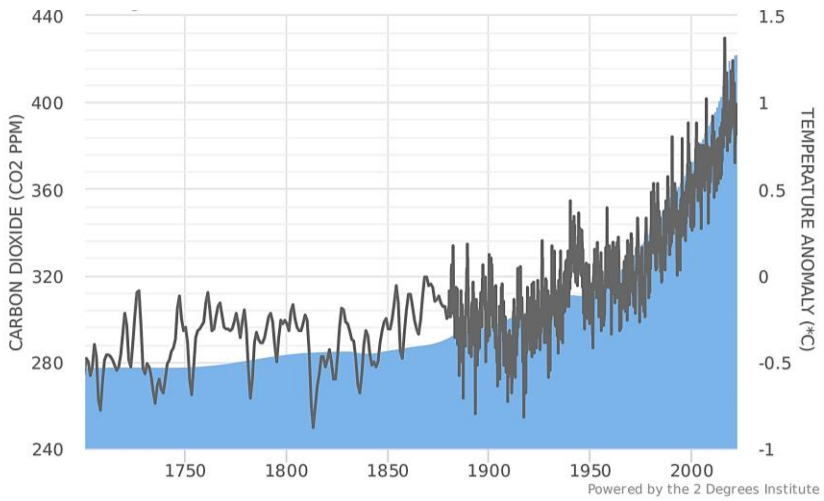

Figure 1: Global CO_2 levels and the effect on temperature; extracted from [3].

In 2019, fossil fuels were the main source in the global primary energy consumption, 78.9 % (30.9 % from oil, 25.3 % from coal and 22.7 % from gas), followed by traditional biomass (6.4 %), hydropower (6.0 %), nuclear (4.0 %), wind (2.0 %), solar (1.0 %), modern biofuels (0.7 %) and lastly other renewable energy sources (including geothermal, biomass, wave and tidal, 0.9 %) [4]. As a result, the world must move away from fossil fuels toward a low-carbon energy mix dominated by renewable technologies and nuclear power. The EU alone aims at reducing 55 % of the GHG emissions of by 2030 and reaching neutrality by 2050; residential and transportation sectors account for almost half of the world's CO_2 emissions [5]. The world needs a disruptive technology to quickly decarbonize the energy sector; the success of this technology critically depends on its social acceptance, sustainability, low-cost and fast implementation.

The Age of Energy Gases (Figure 2) illustrates the sources of energy used throughout the years since the 19th century. It is clear a change in the global energy economy paradigm, with the increased usage of natural gas, methane (planet's most abundant and cleanest hydrocarbon) and hydrogen, followed by the displacement of solid coal and, subsequently, liquid oil [6]. There is then the need for an energy carrier that can be cost-efficiently transported and stored to deliver renewable energy from good remote resource areas, at the right time and place to the energy demand. Hydrogen is emerging to decarbonize the energy sectors, namely industry, mobility, electricity balancing and heating.

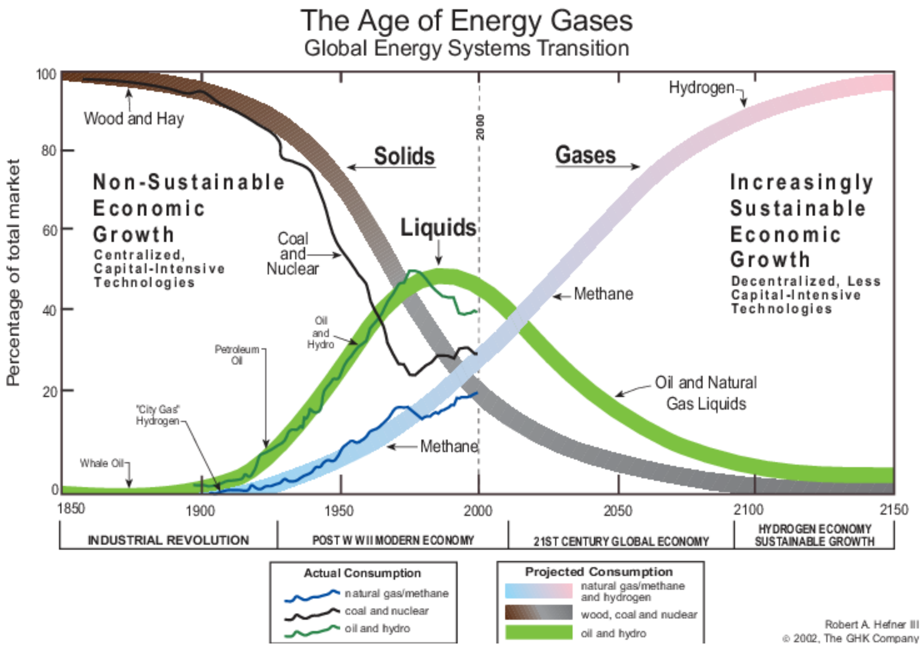

Figure 2: World's primary energy substitution based on the Age of Energy Gases evolution; extracted from [6].

Figure 3 shows a schematic of the future "hydrogen economy" scenario. All aspects of the hydrogen economy must be handled at the same time, including production, storage, transportation, and distribution, while strategic policy support must be maintained. According to a growing number of reports, hydrogen has the potential to play a key role in almost every aspect of the energy system (electricity generation and transportation), and energy system-level assessments show hydrogen to be a technically and economically viable option for energy transition [7], [8]. Green hydrogen, produced by water electrolysis systems with the surplus electricity from renewables, is expected to replace fossil electricity generation currently used to compensate load fluctuations in electrical grids and to serve as a valuable chemical stock in industries of steel, ammonia, petrochemistry, *etc*.

Hydrogen distribution and storage infrastructures are still not present. Blending hydrogen with natural gas in current gas distribution systems is seen a first step to serve as supply chain of hydrogen production plants; many countries have started to do it. A pure and low-pressure hydrogen transport is possible with polyethylene pipes [9]. Adaptions to the gas infrastructure will be then done without major changes while both production and demand are constantly increasing with the phase-out of fossil fuels. Nowadays, hydrogen is already shipped and commercialized in any place in the world. This trend will dramatically increase in the coming decades and many other options will be developed depending on the application. Hydrogen can also be used in combustion or turbines to produce heat, electricity, or mechanical power. However, electrochemical conversion via fuel cells is becoming mainstream in applications for industrial, residential and transport sectors.

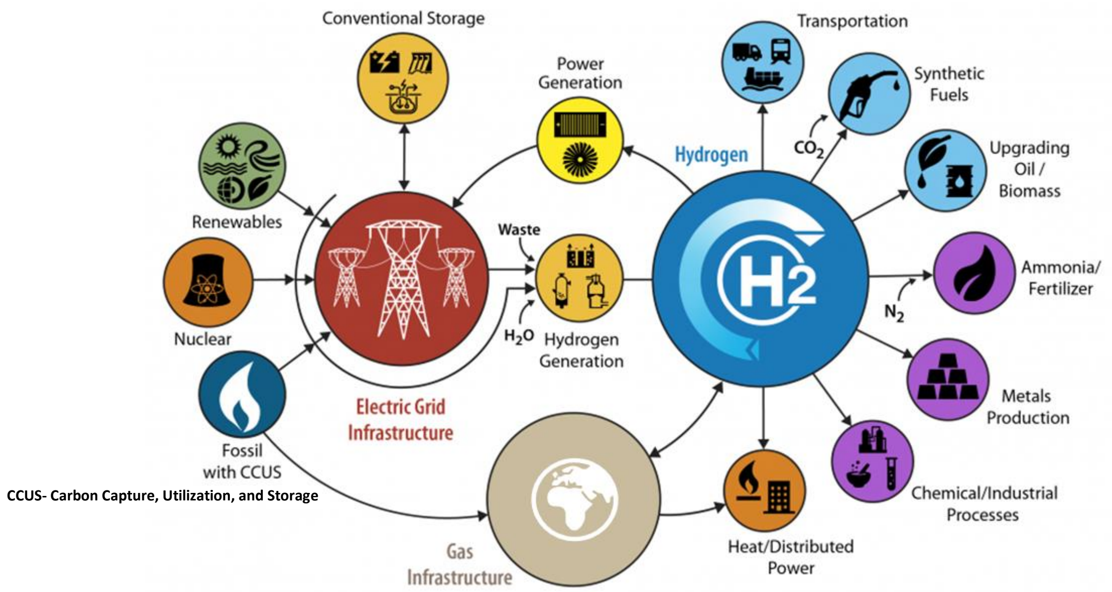

Figure 3: Hydrogen Economy; adapted from [10].

Today, industrial applications account for the majority of the 60 million tons of hydrogen produced globally each year. There are many forms of storing and transporting hydrogen such as pressurized hydrogen, liquid hydrogen carriers (methanol, ammonia, *etc*.) or in the form of metal hydrides. In fact, the majority of hydrogen (53 %) is utilized for ammonia production (that is mostly used for nitrogen fertilizers), followed by the oil sector and methanol synthesis (40%) and polymer and resin manufacture (7 %) [11]. Hydrogen is used in the oil industry to refine crude oil via hydrocracking and hydrotreating, as well as to remove sulfur from diesel and petrol transportation fuels to comply with fuel quality regulations. In current refineries, hydrogen generation accounts for around 5 – 20 % of overall refinery emissions. These industries can use cheap and relatively impure hydrogen, derived mostly from reforming of fossil fuels. Decarbonizing hydrogen generation can drastically lower the carbon footprint of fuels and manufactured goods with such high levels of use in high-carbon-intensity industries [12].

Transportation is responsible for over a quarter of worldwide CO_2 emissions and unless new measures are implemented, global transportation activity is expected to duplicate by 2050 [13]. One solution that can potentially overcome this issue is hydrogen moved cars, that produce no air pollution and have zero carbon impact at the point of use. Toyota, Honda, and Hyundai have already begun to release hydrogen-fueled Fuel Cell Electric Vehicles (FCEVs) into the market, with an initial promise to create vehicles in the low thousands each year, with the main costs being attributed to the fuel cell powertrain and the hydrogen storage system [14]. Furthermore, most vehicles in the maritime and rail industries are still in their the proof-of-concept stage [15].

Although decarbonizing heat has received far less attention in the past than electricity sector, there is now widespread recognition of the need to replace current hydrocarbon fuels used for heat generation with low-carbon alternatives, starting with natural gas. Converting the gas network to hydrogen, on the other hand, might deliver low-carbon heating that is less disruptive to consumers and potentially cheaper than the existing options. Blending hydrogen with natural gas could be a first step toward converting the gas infrastructure to transport hydrogen exclusively and many countries have started to do it. A pure and low-pressure hydrogen transport is possible with polyethylene pipes [16].

Current worldwide hydrogen production (*ca.* 95 %) comes from a process called steam methane reforming that is still generating unacceptably significant quantities of GHG. Water electrolysis using renewable electricity allows producing green hydrogen, but it is still too expensive (3 - 4 times). Catalytic methane decomposition (CMD) has emerged as a disruptive technology to produce clean hydrogen from natural gas or biogas at low temperatures (500 – 650 ºC). Solid carbon is a by-product of this process, which tends to grow over the catalytic surfaces, deactivating them, and causing reactor clogging, which leads to reactor shutdown. Therefore, the catalytic membranes are one of the main components of the CMD reactor and increasing their activity, as well as, understanding the solid carbon production phenomenon, is of major importance. The present dissertation aims at contributing to the scientific efforts of developing innovative and Earth-abundant catalytic membranes that could bring CMD closer to practical applications. Successive Ionic Layer Adsorption and Reaction (SILAR) technique was used to deposit catalytic membranes based on NiO thin and conformal films, demonstrating unprecedented catalytic activities for hydrogen production from CMD.

1.2 Presentation of the company

Pixel Voltaic (https://pixelvoltaic.com/) is a spin-off company from the University of Porto (UPORTO), founded in 2018, for producing renewable energy related technologies, aiming at reaching the proof-of-concept to an industrial level and the market. This company was originally created focusing on the development of engineered solutions for photovoltaic solar cells, namely the low temperature, laser assisted process to hermetically seal glass substrates, a unique process quite relevant for encapsulating Dye Sensitized Solar Cells (DSSCs), Perovskite Solar Cells (PSCs), and Organic Photovoltaic (OPV) cells. In 2019, the corporation expanded its business model through the demonstration of a new process for clean hydrogen production from catalytic methane decomposition. Pixel Voltaic, together with UPORTO, owns a patent for clean and inexpensive hydrogen production, which is expected to enable a smooth and swifter energy transition. Hydrogen produced will supply current needs (use in petrochemistry, ammonia and steel production) and provide a flexible solution to accelerate the electrification of the energy sector in residential, industrial and transport applications.

The present work was performed in collaboration with the Laboratory for Process Engineering, Environment, Biotechnology and Energy (LEPABE). LEPABE, as an interdisciplinary group, is today the largest research unit operating within the Faculty of Engineering of the University of Porto (FEUP) in the fields of Chemical, Environmental and Biological Engineering. LEPABE is classified as “Excellent” by the various international evaluation panels appointed by the Science and Technology Foundation (FCT). “From Science to Innovation” is the LEPABE’s slogan that has been enforced by the combination of basic science with applied engineering and innovation investing in scientific research and technological development, as well as in advanced training, technology transfer and stimulating the establishment of new technology-based companies. LEPABE's scientific architecture comprises three main areas: 1) Environment and Health; 2) Energy, Processes and Products; 3) Biotechnology and Interfaces. The present work aims at the area (2) led by Professor Adélio Mendes, who directs research laboratories at the Chemical Engineering Department of FEUP and at Science and Technology Park of the University of Porto (UPTEC), where are Pixel Voltaic’s offices.

UPORTO-LEPABE is leading the European Project 112CO2 (https://www.112co2.eu/) aiming at low-temperature catalytic methane decomposition for hydrogen production; Pixel Voltaic is responsible for the system integration and technology demonstration and upscaling. The project is composed of seven consortium partners: three universities, one research center, two companies and one SME from five countries and one EU-associated country (Figure 4) [17].

Figure 4: European Project 112CO2 - Consortium Partners.

1.3 Contribution of the author to the work

Currently, 80 MT of grey hydrogen (with CO_2 emissions) are produced annually to supply the industries of petrochemistry, ammonia and steel, mainly through Steam Methane Reforming (SMR). Catalytic methane decomposition is an alternative process for producing low-cost COx-free hydrogen. The methane decomposition of natural gas is expected to play a major role for a swift decarbonization of the energy, since it can use the whole natural gas infrastructure. Also, the produced hydrogen is expected to be *ca.* 30 % cheaper than that from the SMR.

The low-temperature catalytic methane decomposition run in a membrane reactor, with cyclic regeneration of the catalyst, is expected to be very cheap, very compact, and reliable technology, using abundant and low-cost materials. However, this technology is still in an early stage – TRL 3. The work developed in this dissertation aimed at the preparation of nickel-based catalyst using Successive Ionic Layer Absorption and Reaction (SILAR) method, which was not reported yet for these applications, neither at Pixel Voltaic nor at LEPABE research group. The assembling of the SILAR deposition setup, the preparation and characterization of the catalyst, as well as the interpretation of the results were some of the tasks under my responsibility.

1.4 Organization of the dissertation

Chapter 1 addresses the current issues surrounding climate change, integration of renewable energies into the grid and the key role of hydrogen for decarbonizing the energy sector.

Chapter 2 presents the technologies available nowadays for hydrogen production, being the potential of catalytic methane decomposition highlighted due to its reliability and cost-effectiveness. The CMD working principles, the advantages/obstacles and all the relevant aspects, such as the reactor design, and the catalysts properties were discussed. Special attention was given to the SILAR technique, since it was the method chosen to the preparation of the catalytic membranes.

Chapter 3 describers the entire experimental procedure of the laboratory work performed, and all the equipment utilized.

Chapter 4 covers and discusses the main results obtained from the variation of condition of SILAR deposition, characterization of the catalyst (SEM and ICP) and the catalytic tests.

Chapter 5 describes the main conclusions taken from the work performed during this dissertation.

Chapter 6 highlights the main objectives accomplished from this project.

2 Context and State of the Art

2.1 Production of Hydrogen

The serious environmental issues associated with the fossil fuels consumption have speeded up the adoption of renewable energy sources mainly wind turbine, solar photovoltaic and hydrogen. Hydrogen is the most abundant element in the universe, but it is not naturally available in its pure form. The main source of hydrogen, nowadays, is methane (CH_4), and the main production process is the Steam Reforming of Methane (SRM), which is responsible for *ca.* 95 % of the hydrogen produced worldwide.[15] SRM consists in the reaction of methane (mainly from natural gas, but also from biogas) with water vapor to produce CO_2 and H_2 (eq. 1), the outlet stream is normally purified to obtain a pure hydrogen current. This process releases *ca.* 700 MT of CO_2 every year to the atmosphere, which increases the final costs of production, and therefore the selling price of H_2 [18].

$$\mathrm{CH_4(g) + \ 2\,H_2O\,(g) \rightarrow CO_2(g) + 4\,H_2(g)}\ , \quad \Delta H^0_{298\,\mathrm{K}} = \ 165\ \mathrm{kJ\ mol^{-1}} \tag{1}$$

Well-established industries like petrochemistry, ammonia and steel production are already pursuing to decrease carbon footprint by using clean hydrogen that needs to be at the same time inexpensive. These are the major challenges, along with the storage issue.

Water electrolysis, also known as electrochemical water splitting, is the alternative process used for producing hydrogen. However, despite it has been studied and exploited extensively since its discovery in 1789, hydrogen produced by electrolysis accounts only for 2 % of all produced molecular hydrogen. Proton exchange membrane (PEM) electrolysis is a promising technology for coupling renewables with hydrogen due to ability to operate with dynamic loads thanks to fast response times [19]. In particular, the compact system design, easy maintenance, low gas crossover are advantageous features comparing to the mature alkaline electrolysis technology [20]. In what concerns the working principles, water electrolysis relies on two half-cell reactions, as shown in Figure 5, namely cathodic hydrogen evolution reaction (HER) and anodic oxygen evolution reaction (OER) for hydrogen and oxygen production, respectively. It is a well-developed and flexible technique, already commercially available, which generates hydrogen with high-purity (*ca.* 100 %) (eq.2 and eq. 3) [21].

$$\mathrm{2\,H_2O\,(l)\ \rightarrow O_2(g) + 4\,H^+(aq) + 4\,e^-}\ , \quad E^0_{\mathrm{ox}} = -1.23\ \mathrm{V} \tag{2}$$

$$\mathrm{2\,H^+(aq) + 2\,e^- \rightarrow\ H_2(g)}\ , \quad E^0_{\mathrm{red}} = 0.00\ \mathrm{V} \tag{3}$$

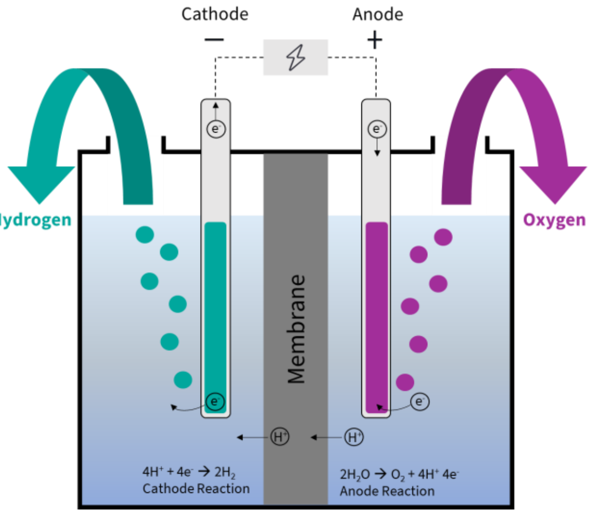

Figure 5: Scheme of the Water Electrolysis Reaction; extracted from [22].

Using the current energy mix for producing electricity, water electrolysis releases *ca.* 25 kg of CO_2 per kg of hydrogen produced. Therefore, green hydrogen generation, *i.e.* with zero CO_2 emissions, is only possible by renewable-powered electrolysis, which is still too expensive (3-4 times). Moreover, scale-up is yet challenging, with hydrogen production costs of 2.3 – 4.6 € kg_{H2}^{-1} from wind and 3.2 – 6.4 € kg_{H2}^{-1} from solar energy, namely using photovoltaic-driven electrolysers [23]. Alternatively, photoelectrochemical (PEC) water splitting devices can be used to produce green hydrogen. Despite PEC cells are a more simple concept, which combine solar collection and water electrolysis in a single device, it is a less mature technology and the hydrogen production costs are higher [24].

Comparing the SRM and renewable-powered electrolysis processes, there are some main differences: i) water electrolysis can operate between 50 °C and 80 °C, while SMR requires high temperatures between 700 °C and 1100 °C; ii) SRM of natural gas has a thermal efficiency between 70–85 %, while electrolysis of water is 70–80 % efficient (*ca.* 20 – 30 % conversion loss), but it is expected to reach 82–86 % before 2030; and iii) hydrogen production cost from SRM is between 1 - 3 € kg_{H2}^{-1} including CO_2 sequestration, and it ranges between 3 - 15 € kg_{H2}^{-1} from water electrolysis (depending on the size of the electrolysis system) [20].

2.2 Methane Decomposition

Alternative, cost-effective, hydrogen production processes without releasing GHG emissions are required. Methane decomposition (MD, eq. 4), also known as methane pyrolysis, consists of cracking the methane molecule, producing solid carbon and clean hydrogen with high purity.

$$\mathrm{CH_4\,(g)} \leftrightarrow \mathrm{C(s)} + 2\,\mathrm{H_2\,(g)}\,, \quad \Delta H^0_{298\,\mathrm{K}} = 74.9\ \mathrm{kJ\,mol^{-1}} \tag{4}$$

The MD process has the unique feature of being a 100 % selective reaction; this characteristic reduces many of the downstream and upstream processes since the gaseous outlet stream contains only hydrogen and unreacted methane. Figure 6 shows the equilibrium conversion of MD with temperature and pressure. According to the source of methane, *i.e.* from natural gas and bio or synthetic methane, the process can become even more environmentally friendly. Apart from allowing the swift decarbonization of the energy, when biomethane is used, this reaction has the power to remove CO_2 from the atmosphere as it produces hydrogen at very competitive costs [25].

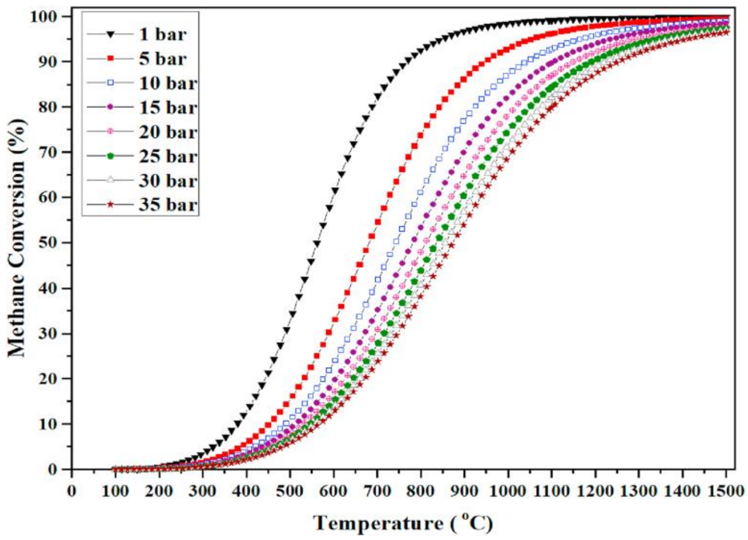

Figure 6: Equilibrium conversion of methane decomposition with temperature and pressure; extracted from [26].

This technology enables using the present storage and distribution infrastructure for natural gas and produces hydrogen to be used locally as a fuel for electricity/heat or as feedstock for chemical industries (steel production, ammonia synthesis, reversal petrochemistry, *etc*.). The costs of operation are projected to be greater than methane steam reforming (1.7 - 1.85 € kg_{H2}^{-1}), but hydrogen is easily purified (methane is the only other gas taking part in the reaction). In contrast to reforming procedures, where secondary products are gaseous, toxic (especially for fuel cells), difficult to separate, and contribute to GHG, in this case, the only secondary product is solid carbon. Since MD is an endothermic reaction, its energy requirements can be combined with the heat released by fuel cells or the "Sabatier" reaction, resulting in increased total energy efficiency. Moreover, the strong binding energy of C-H bonds (440 kJ mol^{-1}) makes it so kinetics and only favorable for temperatures higher than 1300 °C. Such high temperatures are highly detrimental to the cost-effectiveness of the process, but catalysts can be employed to reduce operation temperatures to 450 - 850 °C [23].

2.2.1 Low Temperature Catalytic Methane Decomposition

Catalytic methane decomposition (CMD) avoids the excessive thermal decomposition requirements, but low catalyst stability is observed due to carbon coverage of the active sites of the catalyst. Furthermore, this carbon by-product can also cause reactor clogging, which leads to reactor shutdown, even in uncatalyzed systems. To solve this issue, techniques to regenerate catalyst particles and safely remove carbon allotropes from the reaction zone must be developed and optimized. Therefore, the development of highly active catalysts that can sustain longer activity, despite massive carbon deposition, optimal experimental settings, and the construction of appropriate reactors are required for the low-temperature methane decomposition process. The properties of the carbon by-products can diversify depending on the conditions and the structure of the catalyst and are extremely important for a low-temperature process, since they influence the overall product yield, and may reduce the final selling price of the hydrogen produced. The catalyst stability is then directly influenced by the growth process for carbon particles, which is dependent on several factors including the catalyst itself, reaction temperature, gas partial pressures, and reactor design.

The CMD working principles are the following. First, methane molecules chemically adsorb on the active phase of the catalyst, which is subsequently removed through the sequential cracking of four C–H bonds. The unattached hydrogen atoms are combined to form molecules, *i.e.* the gas phase product. Then, carbon nucleation occurs, resulting in the formation of carbon nanofilaments on the catalyst particle's trailing face. In the end, atomic carbon aggregates each other to form encapsulated carbon [25].

At the beginning of the 20th century, the first publications on catalytic methane decomposition (CMD) were published. Among the materials studied, Slater found iron and charcoal to be the most effective catalysts (silica, alumina, magnesia, lime, barium oxide, wood charcoal, graphite, silicon carbide, iron, and copper) [27]. The number of publications regarding CMD increased exponentially in the 90s, with a heightened focus on the reaction mechanism. Some authors still believe the reaction starts with a methyl radical, which leads to multiple chain reactions and the formation and consumption of C2–C6 hydrocarbons; while others believe the reaction starts with methane adsorption on the catalyst surface, followed by stepwise dehydrogenation and hydrogen desorption, and then carbon diffusion and deposition. Although there is no unanimous agreement on the mechanism, the latter has steadily gained more acceptance [23].

By the end of the 20th century, extensive research has started thinking on the CMD process for producing clean hydrogen. In 2001, Muradov *et al*. proposed the use of the methane decomposition reaction for decarbonization of the energy sector [28]. CMD displays very high selectivity, and the product gas stream contains only hydrogen and unreacted methane, complying with standard ISO 14687, which requires CO concentration lower than 0.2 ppm [29]. However, the CMD processes displayed very low stability, just a few hours on stream, and moderate catalytic activities, in the range of 1 $g_{H2}\ g_{Cat}^{-1}\ h^{-1}$. For producing clean hydrogen with the required purity and quantity for the envisioned hydrogen economy, the stability of CMD catalysts became the main topic of research since then.

2.2.2 Catalysts

2.2.2.1 Metal Catalysts

Metal catalysts are the most used materials for the CMD reaction. Because of their partially filled 3*d* orbitals that allow electron acceptance, transition metals are known to be the most active materials for the dissociation of hydrocarbons. Noble metals, namely platinum and palladium, were utilized as promoters in other attempts to improve the effectiveness of CMD catalysts, but the associated capital costs make their use impractical [23]. For this reason, more Earth-abundant materials like nickel, iron, and cobalt, which are very active, are thought to be the best metals for producing hydrogen from CMD. Numerous investigations on CMD using a Ni-based catalyst have been conducted since Ni is recognized to be a favorable active metal in this catalytic process because of its low cost and effectiveness in the reaction [30]. Although showed higher activities, they are unstable at temperatures higher than 650 °C, whereas iron and cobalt-based catalysts, despite their lower activity, can be used at higher temperatures and create better-value carbon. Manganese, molybdenum, tungsten, and most noble metals are also commercially employed to decompose methane, but only on a limited scale because of their low carbon solubility leading to rapid carbon deposition and catalyst deactivation [23].

Despite efforts to increase the activity and stability of monometallic catalysts, deactivation by coke production has not been solved for pilot or industrial scales. As a result, different metals began to be combined, resulting in the creation of the second generation of catalysts. The mix of nickel with iron or copper received the most attention among the potential metal combinations. Table 1 compares many of the most effective metal catalyst combinations reported to date, considering: metal molar composition (predominant metal, chemical promoter, support), reaction temperature (T), catalyst shape, particle diameter (d_m), methane feed, average activity (a), average conversion (X_{CH4}), and time-on-stream (t).

Table 1: Comparing bi- and tri-metallic metal catalysts for CMD; adapted from [23].

Catalyst	T / °C	Catalyst shape	d_m / nm	Feed / $g_{CH4}\ g_{cat}^{-1}\ h^{-1}$	a / $g_{H2}\ g_{cat}^{-1}\ h^{-1}$	X_{CH4} / %	t / h
75Ni-15Cu/Al_2O_3	625	n/a	20-25	64.29	3.241	20	54
82Ni-8Cu/Al_2O_3	625	n/a	20-25	64.29	2.791	17	62
62Fe-8Ni/Al_2O_3	625	n/a	25-50	32.14	0.755	22	64
50Ni-25Fe/Al_2O_3	650	Fine powder	40	8.58	0.892	42	>210
60Ni-25Cu/SiO_2	650	Fine powder	9	64.29	5.333	33	30

24Ni-6Cu/MgO	665	Fine powder	38	51.43	3.378	26	45
15Fe-3Ni/MgO	700	Fine powder	3	2.14	0.386	72	3
30Fe-15Co/Al_2O_3	700	Slab	5-40	2.14	0.380	71	3
30Fe-10Ni-5Co/Al_2O_3	700	Slab	5-40	2.14	0.375	70	3
15Fe-6Co/MgO	700	Fine powder	3	2.14	0.375	70	3
15Fe-6Mn/MgO	700	Fine powder	5	2.14	0.375	70	3
30Fe-5Ni-10Co/Al_2O_3	700	Slab	5-40	2.14	0.370	69	3
30Fe-7.5Ni-7.5Co/Al_2O_3	700	Slab	5-40	2.14	0.359	67	3
25Ni-25Co/SBA-15	700	Fine powder	20	3.57	0.171	19	5
50Ni-10Fe-10Cu/Al_2O_3	750	Slab	20	2.57	0.521	81	10

Ni-Fe catalysts can maintain activity at higher temperatures than Ni-based catalysts alone. When Ni is used as the predominant metal, the new structure consists of a Ni-Fe alloy, with no reported evidence of metallic iron. Increasing the concentration of Fe to a Ni-based catalyst enhances stability until an optimal composition. Wang *et al.*[31] used a bimetallic Ni-Fe alloy supported in Al_2O_3, with a molar ratio of 2Ni:1Fe:1Al, for performing the CMD reaction at 650 °C. They reported a stable activity of *ca.* 0.9 $g_{H2}\ g_{Cat}^{-1}\ h^{-1}$ during 210 h, which was attributed to the enhanced ratio between atomic carbon diffusivity through the catalyst particle and reaction rate, by adding Fe, as a chemical promoter; in pure Ni, at high temperature, methane cracking is faster than carbon diffusion, causing carbon accumulation at the catalyst surface (encapsulation/deactivation). On the other hand, Ni-Cu catalysts are able to achieve the highest activity among all catalysts tested, as shown in Table 1. In most catalysts, for higher activities, stability is frequently very low, in the range of 3-5 h: with this type of Cu doped Ni-catalysts, more than 20 h on-stream are often observed [32]. Shen and Lua tested carbon nanotubes (CNT) as a support for Ni-Cu catalysts and obtained a maximum activity of *ca.* 4.4 $g_{H2}\ g_{Cat}^{-1}\ h^{-1}$ and 30 h on stream, using a Ni-Cu/CNT catalyst at 700 °C [33].

2.2.2.2 Carbon catalysts

Carbon materials have been studied as catalysts for CMD because they are less expensive and less poisonous than metals, such as activated carbon and carbon black. The activation energy of activated carbon and carbon blacks (between 100 - 300 kJ mol^{-1}), on the other hand, is much higher than that of metals (65 – 75 kJ mol^{-1}) [23]. Carbon catalysts are often utilized at temperatures exceeding 750 °C to achieve considerable activity. When operating at these high temperatures, carbon catalysts are more stable than metal catalysts. However, they are also more difficult to regenerate without causing damage to the catalyst, which makes them less suitable for long-term use.

2.2.2.3 Synthesis method and catalyst supports

Beyond the materials employed in CMD, the synthesis process plays a big role in catalyst optimization. To maximize the lifetime of catalysts, many synthesis procedures have been tried, *e.g.*, impregnated, co-precipitated, and fused catalysts boosted hydrogen production in that sequence; particle size increased in the reverse order [34]. The size of the particles in a catalyst affects its activity and the mechanism by which carbon materials are formed. When examining different loadings of metal in a Ni/SiO_2 catalyst, Wang *et al.*[32] reported that particles with a size between 10-100 nm produced carbon nanofilaments and smaller particles (< 10 nm) produced amorphous carbon that rapidly encapsulate the metal particle. Takenaka *et al.*[35] also reported that particles with a diameter of 60 nm to 100 nm had the longest lifespan during the CMD reaction. Calcination and reduction procedures are required for the creation of supported metal catalysts. The temperatures used in these methods have a significant impact on the catalyst properties, particularly in terms of particle size and metal-support interaction. The method chosen to prepare the catalyst has an effect on the dispersion of Ni on the support, which influences the catalytic activity in methane decomposition.

The type of catalyst supports is one of the key factors affecting the catalytic activity in CMD, namely the loading and size of metallic particles and on the metal-support interaction. The correct interaction between an active metal and the catalyst support is the most important component in catalytic activity. To promote improved dispersion of the active phase, the ideal support should have advantageous features, such as chemical and mechanical resistance, as well as a large surface area. Because of the correct interaction between metals and supports, CMD is improved, and catalysts become extremely refractory and stable in sintering and coke production. The most used catalyst supports are metal oxides of Al_2O_3 or SiO_2, although MgO, CeO_2, and TiO_2 are also used [30]. Takenaka *et al.*[36] tested several supports (SiO_2, TiO_2, graphite, ZrO_2, $SiO_2{\cdot}Al_2O_3$, Al_2O_3, $MgO{\cdot}SiO_2$, MgO), and reported that SiO_2, TiO_2 and graphite are the supports with the highest carbon yields at 500 °C (199 $g_C\ g_{Ni}^{-1}$, 136 $g_C\ g_{Ni}^{-1}$ and 114 $g_C\ g_{Ni}^{-1}$, respectively). The authors attributed the lower activity to the formation of highly stable support phases with NiO during calcination, making the latter harder to reduce. In a similar work, SiO_2 supports were tested with different pore structures. SiO_2 with wider pores yielded the highest activity, of *ca.* 0.5 $g_{H2}{\cdot}g_{Cat}^{-1}{\cdot}h^{-1}$ [35]. This result suggests that pore size and volume of the catalyst support are critical parameters for the growth of carbon structures, as small-sized pores get easily clogged.

2.2.3 Deactivation

Any catalyst employed for methane decomposition, is expected to become deactivated over time because of carbon deposition (site-blocking) or accumulation at the entrance of the pores. The particles need to have their active sites available to adsorb the reagents and then complete the reaction; being the carbon formed in the solid state, the base of the structure will be on the exact active site. The amount of carbon and its structure clearly depend on the temperature and the catalyst used and, therefore, the time needed for stopping the CMD reaction is variable [37]. The carbon deposits can grow over the catalyst - base-growth phenomenon, or between the catalyst and the support - tip-growth phenomenon - Figure *7*.

When the catalyst-substrate interaction is weak, as shown in Figure *7* (a), (the metal has an acute contact angle with the substrate), hydrocarbon breaks down on the metal's top surface, carbon diffuses through the metal, and CNT precipitates out across the bottom of the metal, pushing the entire metal particle off the substrate (step i). CNT extends further and further as long as the metal's top is accessible to the decomposition of incoming hydrocarbons (ii). When the metal is completely covered in extra carbon, the growth of CNT is interrupted (iii). The "tip-growth" refers to this. When the catalyst-substrate interaction is strong, as shown in Figure *7* (b), early hydrocarbon breakdown and carbon diffusion occur similarly to that in the tip growth case, but the CNT precipitation is unable to raise the metal particle, forcing it to emerge from the metal's apex. Carbon begins to grow as a hemispherical dome of carbon, which then grows upward in the shape of a smooth graphitic cylinder (i). Afterwards, when the dissolved carbon diffuses upward, hydrocarbon is deposited on the metal's lower peripheral surface (ii). This is referred to as a "base-growth" [38].

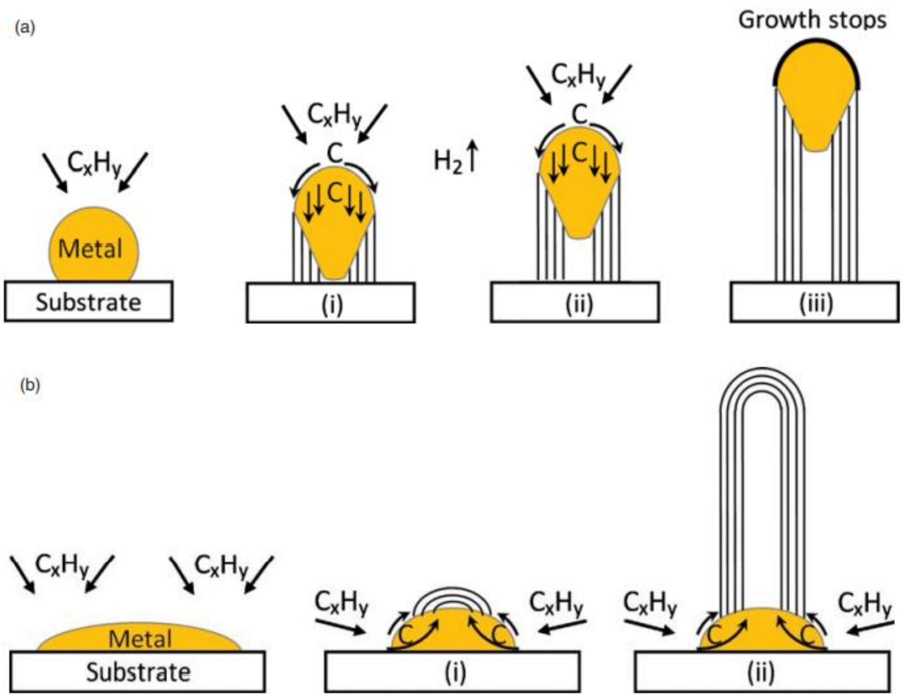

Figure 7: Mechanism of the formation of nanocarbon tubes in the Ni-catalyst: a) tip-growth b) base-growth; extracted from [38].

In some cases, when the catalyst-substrate interaction is intermediate, a mix mechanism of the formation of CNT can occur. As the CNT grow, the portion in touch with the Ni particle narrows, and the metal particle's tail is dragged inside the carbon capsule, forming a small piece of Ni particle contained in the carbon tube with a diameter equal to the carbon tube's inner diameter, as shown in Figure 8. Each filament has a bright tip, identified to be a nickel particle. The presence of small fragments of Ni particle in carbon nanotubes may be dependent on the reaction temperature and degree of contact between Ni particle and support. Higher reaction temperatures usually favor the formation of carbon tubes embedding small pieces of Ni. If the Ni particle is deeply rooted into the support, only a small portion of the surface is exposed to the reaction atmosphere, the interaction between Ni particle and support is strong, so the formed carbon nanotubes do not embed any pieces of small Ni particles [39].

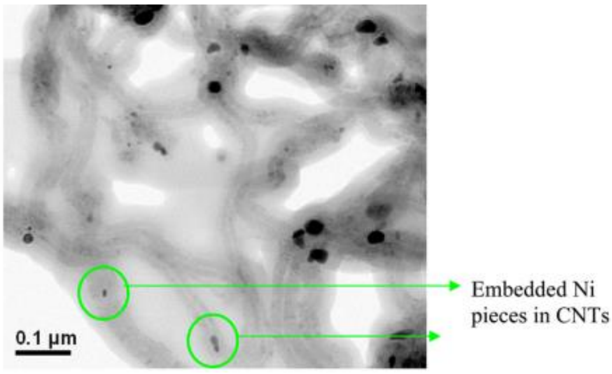

Figure 8: TEM micrographs of the carbon nanotubes (CNT) found in the catalytic evaluation of 50 wt% Ni/Ce-MCM-41-20 after 1400 min of reaction; extracted from [39].

The reaction process can theoretically continue, if subjected to regeneration of the catalyst. But when the CNT formed is tip-grown, carbon separates the catalyst from the support and, as such, turns the catalyst regeneration impossible. In that case, the catalyst particles will progressively detach from the support and be removed along with the formed carbon. Therefore, regeneration is possible, and may theoretically allow the process to go-on indefinably, as long as the deposits are base-grown. A gasifying agent must directly gasify the carbon deposits and/or the CMD catalyst should catalyze the gasification [40].

2.2.4 Regeneration

The replacement of the inactive particles after every cycle of production is not sustainable and practical for large-scale applications. Therefore, the catalyst needs to be subjected to a regeneration process that can be proceeded by three simple reactions: combustion, gasification, and hydrogenation. Combustion was the first thought solution to regenerate the covered particles, and the known reaction consists basically in eq.5: [41]

$$\mathrm{C\,(s)} + \mathrm{O_2\,(g)} \rightarrow \mathrm{CO_2\,(g)}\ , \quad \Delta H^0_{298\,K} = -\,393.4\ kJ\ mol^{-1} \tag{5}$$

Since what covers the active sites is solid carbon structures, a simple combustion reaction can be effectively triggered, but since the main objective of this CMD method is to emit zero GHG, it should not be considered. Gasification (eq. 6) is a better alternative since steam can gasify coke, which can be utilized to regenerate the catalyst [42]. Additional hydrogen is produced, increasing the H_2/CO_x ratio of the process.

$$\mathrm{C\ (s) + H_2O\ (g) \rightarrow CO\ (g) + H_2\ (g)}\ , \quad \Delta H^0_{298\,K} = -\ 131.2\ kJ\ mol^{-1} \tag{6}$$

Although these two processes have overall less GHG emissions compared to the typically hydrogen production processes, hydrogenation (eq. 7) comes as an innovative and cleaner approach, promoting the flipside reaction. Because CMD process is reversible, it has been proposed that hydrogen may be utilized to gasify carbon deposits by reversing the CMD reaction [42].

$$\mathrm{C\ (s) + 2\ H_2\ (g) \leftrightarrow CH_4\ (g)}\ , \quad \Delta H^0_{298\,K} = -74.9\ kJ\ mol^{-1} \tag{7}$$

Hydrogen is a weaker gasifier than oxygen, but as hydrogen is a reducing agent; it does not corrode the reduced catalyst. The total amount of hydrogen required for the methanation of the deposited carbon is the same as that used to create the deposits. As a result, the mechanism of regeneration must be localized. Carbon gasification should occur selectively at the interface between the produced carbon structures and the catalyst; Ni has been demonstrated to catalyze both CMD and the reverse process, and non-catalytic gasification is sluggish. Only a percentage of the hydrogen produced must be required to completely remove the carbon materials from the catalyst, as long as there is proper contact between the gas phase and the carbon-catalyst interface. Furthermore, this strategy would allow for an almost full recovery of carbon materials, as only carbon at the catalyst interface is hydrogenated, with the rest being separated from the catalyst. Carbon materials vary considerably depending on operation conditions and catalysts: the most reported carbon products include amorphous carbon (mostly on carbon catalysts) and graphitic nanomaterials (mostly filamentous carbon on metal catalysts) [43]. Although the need for catalyst regeneration can increase operational costs, carbon products can be recovered and exploited for profit, increasing the economic interest of the process. Therefore, hydrogen gasification despite allowing for the design of reactors without any direct emission of greenhouse-effect gases, also allows to reuse the carbon by-product.

2.3 Reactor Design

Alongside with catalyst development to prolong catalyst lifetime, the reactor configurations reported so far still show room for improvement and are equally important for methane decomposition to became attractive at an industrial scale [23]. In the last ten years, a variety of reactors such as fixed bed reactor (FBR), fluidized bed reactor (FLBR), plasma reactor (PR) and molten-metal reactor (MMR) have been studied for CMD [44].

Fixed bed reactors are the most commonly used for methane decomposition process [45]. The drawback with their utilization is the fact that carbon is deposited over the exterior surface of the catalyst particles (Figure 9), therefore clogging the reactor and increasing the pressure drop; these are the main reasons for low performances with FBR. The deposited carbon must be removed on a regular basis to keep the catalyst active and prevent the reactor from clogging [46]. A FLBR provides that solids flow continuously through the reaction zone, making it ideal for the continual removal of carbon particles from the reactor, which may be easily adjusted by altering the ratio between the feed rate and the weight of the bed. However, the pumping requirements (high fluid velocity required to fluidize the bed), the entrainment of particles in the outstream of the reactor and the pressure drop associated are the major drawbacks in a FLBR.

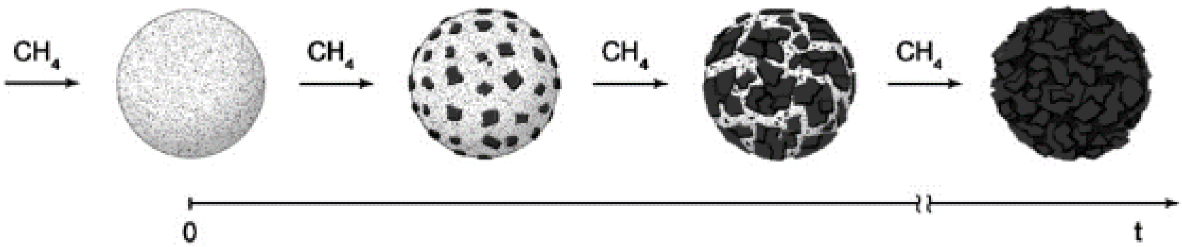

Figure 9: Representation of a catalytic bed particle during CMD; adapted from [47].

Alternative options are the plasma reactor (PR) and molten-metal reactor (MMR). PBRs offer an attractive alternative to traditional catalytic beds. Various configurations, namely, dielectric barrier discharge, corona discharge, glow discharge, microwave, gliding arc, and spark discharge were used to MD. However, the formation of heavier hydrocarbons (mainly C2 and C3), their low selectivity, high power input and therefore the low energy efficiency make this endothermic method less viable. MMR (Figure 10) design was suggested to avoid catalyst deactivation caused by carbon deposition [48], which is characterized by its high operation temperature and the liquid state of the catalyst. Although MMR has the potential to overcome the key issues in CDM, it needs to be operated at temperatures higher than 1000 °C (to melt the catalysts), which affects the implementation of such reactors [49]. To accomplish significant hydrogen production, temperatures around the range of non-catalytic methane decomposition are required, meaning the same disadvantages as pure thermolysis (reactor wear and high energy intensity) [23]. BASF implemented a moving bed reactor with carbon materials operating at 1400 °C, using induction heating. However, this reactor configuration revealed low radial heat transfer and it was reported the need to develop materials for high temperature operation. This implies low energy efficiencies and high wearing and then higher production costs; moreover, it is only suitable for stationary applications [50], [51].

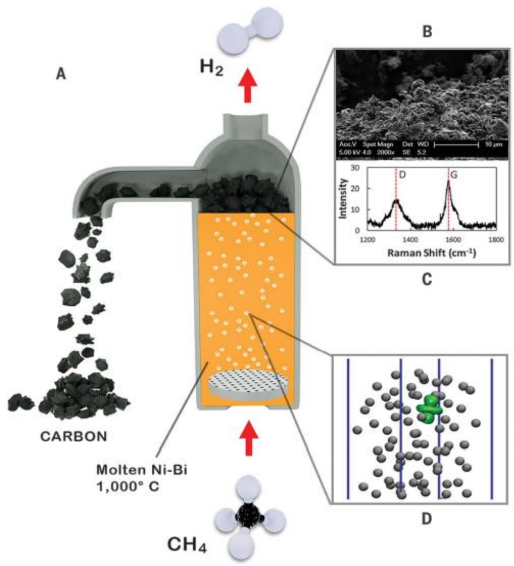

Figure 10: Schematics of hydrogen production with a Ni-Bi molten catalyst – MMR; adapted from [48].

When comparing traditional processes to process integration, which combines reaction and membrane separation in a single unit, there are numerous advantages. In recent years, the membranes can be used in conjunction with a chemical or biochemical reaction to improve the overall process, which results in increased conversion and selectivity, as well as a compact and cost-effective reactor design. Membrane reactors (MRs) are a promising technology in a variety of fields, including pharmaceutical, biotechnology, petrochemical, energy, and environmental applications, as well as phase change behavior [52], [53].

The three main concepts of extractor (that removes the products from the reaction mixture selectively), distributor (controls the addition of reactants to the reaction mixture), and contactor (increases the amount of contact between the reactants and the catalyst) can be used to categorize most of these approaches. Membranes are structures that are permeable to at least one component of the surrounding fluid while impermeable to the other components.

In the low-temperature methane decomposition process, the contactor is the most suitable type of MR, since the membrane by improving the interaction between the reactant and the catalyst the conversion of the reaction would increase. Among the various works focused on applying membrane reactors in various industrial processes, their use at an industrial scale is missing. The main disadvantages are a lack of scientific evidence about the long-term stability of membrane reactors used in real-world operating conditions and a very high fabrication cost [52]. Pixel Voltaic, in collaboration with UPORTO filled the first patent describing the CMD process and the reactor, *i.e.* the low-temperature catalytic methane decomposition run in a membrane reactor at 550 - 650 ºC, with cyclic regeneration of the catalyst [54].

2.4 Catalytic Membranes

Catalytic membranes without a separation function have been used successfully as microstructured reactors. When a reactant combination is forced to flow through the holes of a membrane impregnated with catalyst, the intense contact allows for strong catalytic activity with minimal mass transport resistances [53]. For this process, inorganic membranes are the most suitable ones considering that they can operate at the temperature that the reaction occurs (300 - 800 °C) and in the aggressive chemical environment due to their high chemical resistance. Carbon, silica, alumina, titania, zirconia, zeolite, palladium, silver, and alloy have all been used to create inorganic membranes. Morphologically they can be dense or porous membranes [52].

These ceramic membranes have an asymmetric structure with two or three layers of pore sizes. The first layer serves as a support, while the second layer is fragile and is responsible for the separation or the contact, increasing the amount of contact between the reactants, having a small pore size. As mentioned before, alumina (Al_2O_3), titania (TiO_2), zirconia (ZrO), glass (SiO_2), and combinations of these metal oxides are frequently used as the catalyst supports for ceramic membrane preparation. In some cases, an intermediate layer is deposited to ensure structural compatibility between the two; the ceramic membrane layers are schematically depicted in Figure 11. The separation layer, present in the figure, in non-separative function membranes is called contact layer.

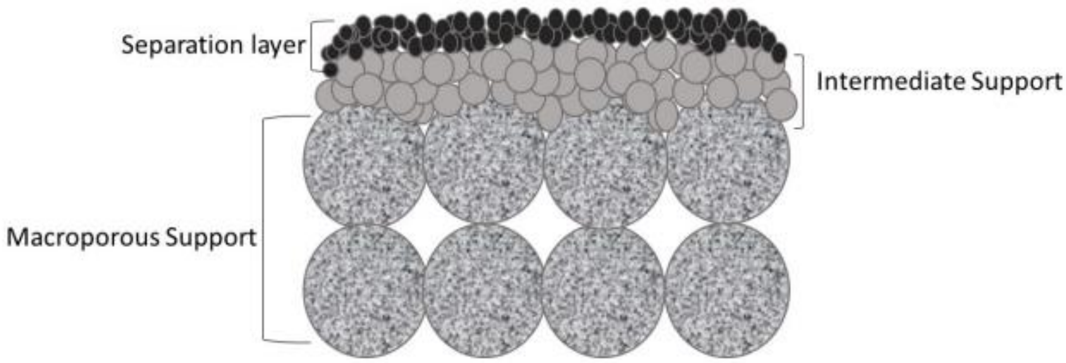

Figure 11: Scheme of ceramic membrane layers; extracted from [52].

Many materials and deposition techniques have been used before finding the most promising catalytic system up to now. Screen-printing, spin-coating, wet spray deposition, and atomic layer deposition (ALD) are the most common methods used. For the deposition of thin and uniform films, successive ionic layer adsorption and reaction (SILAR) is not well studied, but is simple, inexpensive, less time-consuming method, and suitable for large area depositions.

This technique is mainly used for the preparation of semiconductor materials, such as ZnS and CdS, as well as doped, alloyed, or multi-layered quantum dots layers on porous films in a direct and simultaneous way [55]. In spite of its simplicity, SILAR has a number of advantages: (i) it offers extremely easy way to dope film with virtually any element in any proportion by merely adding it in some form of the cationic solution; (ii) unlike closed vapor deposition method, SILAR does not require high quality target and/or substrates nor does it require vacuum at any stage, which is a great advantage if the method will be used for industrial application; (iii) the deposition rate and the thickness of the film can be easily controlled over a wide range by changing the deposition cycles; (iv) operating at room temperature can produce films on less robust materials; (v) unlike high power methods such as radio frequency magnetron sputtering, it does not cause local over heating that can be detrimental for materials to be deposited; and (vi) there are virtually no restrictions on substrate material, dimensions or its surface profile [56]. However, it was never applied for the preparation of catalytic membranes for methane decomposition.

SILAR is a chemical processing method, first developed by Nicolau *et al.* in 1984, which is based on immersion of the substrate into separately placed cations and anions. As it is a chemical method, a large number of varieties of substrates can be coated [56]. The deposition is carried out at or close to room temperature, avoids oxidation or corrosion of metallic substrates. Stoichiometric deposit is easily obtained. Since the basic building blocks are ions instead of atoms, the preparative parameters are easily controllable and better orientation and improved grain structure can be obtained. Basically, this procedure combines two different deposition methods: Atomic Layer Deposition (ALD) and Chemical Bath Deposition (CBD). ALD is capable of producing highly uniform ad conformal thin films and relies on deposition of alternating layers of precursors under controlled vacuum to obtain a homogenous and highly ordered film on the substrate [57]. CBD has been used to deposit thin layers on a substrate in a variety of ways, using a controlled chemical reaction by heterogeneous precipitation [58]. This precipitation formation, *i.e.* wastage of material, is avoided in SILAR method where thin films are obtained by immersing substrate into separately placed precursors and rinsing between every immersion with ion-exchanged water. The rinsing time in ion exchange water is critical for ionic layer formation [56]. The creation of functional devices or a wide range of applications requires methods for fabricating thin films with well-controlled structure and characteristics. Nanometer sized materials have recently attracted considerable attention for their unique physical and chemical properties, having large surface to volume ratio and quantum size effect [59].

A thin film is composed of a single layer or a collection of layers of one or more materials that are deposited on a surface and may be used to change the characteristics of the support substrate or construct a device. Many materials behave differently in film form than in bulk, depending on their morphology, thickness, nano-/micro-structure, and other factors. Still the term "thin" is subjective, they can range in thickness from a single atomic layer to hundreds of nanometers and even a few micrometers, depending on the application [60]. These kind of films are used in a variety of applications, including (opto)electronic devices (transistors, solar cells, and light emitting diodes (LEDs)), paints, functional coatings in the building industry (antireflection, self-cleaning, heat mirrors, and anti-corrosion), and active components in batteries and energy storage technologies in general [61].

For the CMD process, SILAR process is expected to allow the deposition of a 2D thin and conformal film, or an aggregation of nanosized clusters, of Ni-based catalysts. Then, the catalytic membrane, combining the planar substrate and catalyst film, is inserted in the membrane reactor for producing hydrogen.

3 Materials and Methods

3.1 Overview

For the production of the catalytic membranes for the membrane reactor, there are 3 important steps: i) the surface of the substrate, needs to be cleaned and activated, in a step called pre-treatment of the substrate, which includes an ethanol ultrasonic bath and, in some cases, a plasma treatment; ii) the deposition of the catalyst in the substrate, in this work by SILAR method; and iii) the calcination of the membrane to obtain the desired chemical and morphological characteristics (Figure 12). SILAR was chosen to prepare the catalytic membranes and the deposition conditions were varied to study their role in the film properties (SEM and ICP) and the catalytic activity.

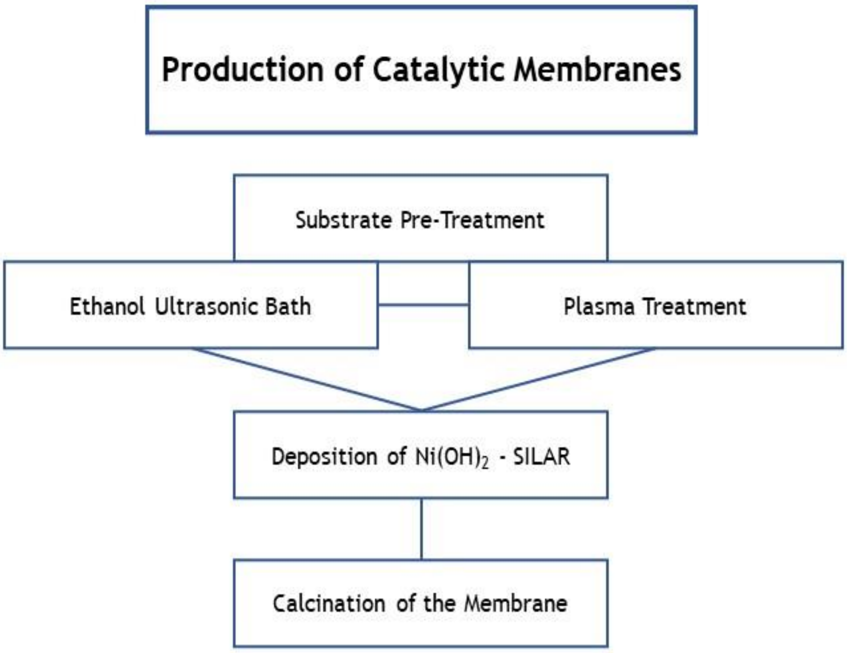

Figure 12: Overview of the Methodology performed for the preparation of catalytic membranes.

For the present work, the catalyst selected was a Ni-based material (NiO), due to the reasons presented in the previous section. Since for this technique, there are cationic and anionic precursors, the cationic precursor is the source of Ni; herein, a solution of 0.1 M $[Ni(H_2O)_2(NH_3)_4]^{2+}$. The anionic precursor, in the other hand, was varied between a solution of NaOH and H_2O_2 with different concentrations. The number of cycles, following the SILAR procedure also varied, between 5 and 40, depending on the anionic precursor and its concentration. The time of dipping was 10 seconds in each solution. The temperature of the solutions where the substrate was dipped were not varied in this study, *i.e.* the temperature of the cationic solution was kept at room temperature (25 °C), while the temperature of the anionic solution varied according to the precursor used (85 °C for H_2O_2, and 25 °C for NaOH).

There are some variables that are binding to the mentioned above, therefore implicit and do not need to be referred in the nomenclature. One of them is the temperature of the solutions where the substrate is going to be dipped. The temperature of the cationic solution was always ambient temperature (25 °C). Meanwhile the temperature of the anionic solution depends on which one is utilized. When is NaOH, the temperature is 25 °C, while when H_2O_2 is used the temperature is 85 °C, sustained by a heating plate.

3.2 Production of the Catalyst

3.2.1 Substrate pre-treatment

An aluminum oxide (Al_2O_3) ceramic substrate (from Kerafol), a disk with an area of 9.62 cm^2, was used to deposit the catalyst films. With the goal of cleaning the substrate of any organic compounds and activate its active sites, the adsorbate is subjected to a pre-treatment before the SILAR deposition method. The substrate was firstly placed in a beaker with a 70 % ethanol solution, which was inserted in an ultrasonic cleaner bath (Figure 13; from VWR, model USC-7) at 50 °C, for 40 min. Following this, the substrate, in certain tests, was submitted to a plasma surface treatment (Figure 14; from Diener, model Zepto), in an air atmosphere, for 30 min. A cold plasma process is a vacuum process that employs reactive species interactions formed at low temperatures. By placing a sufficiently strong electromagnetic field over a gas at low pressure, glow discharges (or cold plasmas) are created. Glow discharge plasma treatment and related procedures are well-established technologies for cleaning and surface treatments. Both equipments are available at LEPABE [62], [63].

Figure 13: Ultrasonic Cleaner USC – VWR.

Figure 14: Plasma surface treatment machine.

3.2.2 SILAR deposition

As mentioned previously, SILAR is a chemical processing method frequently utilized to deposit thin films, which has been receiving huge interest in the scientific community due to its relative simplicity and inexpensive cost. Briefly, the main steps in a SILAR deposition are shown in Figure 15, combining: adsorption of the cations, rinsing, reaction of pre-adsorbed cations with newly adsorbed anions and again rinsing, if needed.

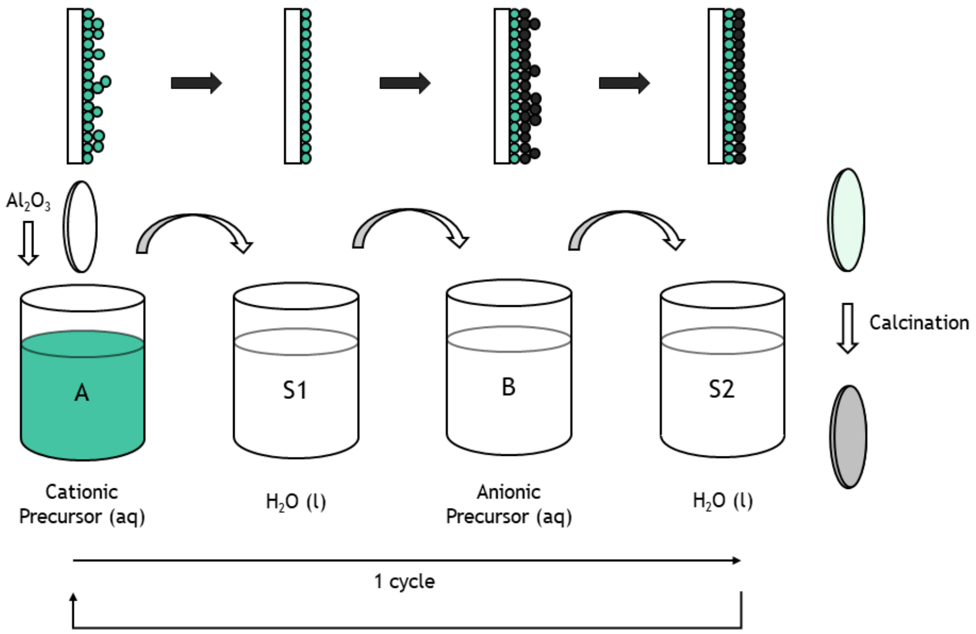

Figure 15: Schematic illustration of SILAR technique.

For the adsorption step, the solution A is the primary ionic solution, usually a metal cationic solution, and the solution B includes the second ionic precursor, usually OH^- for hydroxides/oxides or S^{2-} for sulfides. The rinsing solutions are generally a pure solvent (like deionized water) – S1 and S2. When the substrate is immersed in the solution A, an ionic precursor, a non-homogeneous monolayer is adsorbed on the surface of the substrate. A following dip in a rinse solution S1 allows to wash the excess and unbound ions, forming a practically homogeneous monolayer. Then, the reaction step occurs dipping it in the solution B, with other ionic precursor and opposite charge. A solid and uniform film is formed. The final rinse S2, using the same solution as the initial S1, is performed to remove the excess and unreacted species. This procedure is cyclic and can be repeated several times until the desired amount of deposited material is achieved. Rinsing steps are not obligatory, but they are used to remove surplus material from the substrate after each precursor dipping and to ensure that there is only one ionic layer left before the substrate is immersed in the next solution. Faster but less controlled growth is observed in the absence of rinse treatments. Furthermore, excess precursor trapped on the substrate's surface could be released into the solution containing the second precursor, leading the compound to precipitate inside the solution [61]. The rinsing steps solution are appropriate when strong precursors are used, aiming to prevent excess adsorbed or loosely bounded species, which do not create one ion layers. When weak precursors are used, it is not favorable to do rinse, since the adsorbed species will only be attached to the highly attractive active sites or not attach at all, forming single layers with not very strong bonds. The rinse, in this case, could lead to detachments and then induce the need to raise largely the number of cycles [64].

There are various factors that can change the properties of the deposited film, such as thickness, particle size and morphology of the films, which can be controlled by varying the number of deposition cycles, the time of deposition, bath temperature, pH, and concentration of the precursor solutions. Therefore, the optimal parameters should be determined for each system specifically to the materials and solvents used [65].

Generally, manual based systems have been used to perform these operations in SILAR method. However, during the present work, a programmable robot (Figure 16; F4000N.1 SERIES ROBOT) was adapted to perform the SILAR steps, with determined dipping steps, certain time of reaction and number of cycles that cannot be mistaken or changed in the middle of the procedure. This setup is capable of doing two directional movements. The part of the device that moves by the direction and sense of the red arrows is marked by a red circle. An arm extension was attached to the moving part of the robot in order to be possible to hold membrane throughout the procedure. A defined number of beakers were displayed in a straight line, in a specific order, following the method, and a tweezers holding the substrate is attached to the arm extension. The robot is programmed using a computer to do certain movements, according to the positions of the beakers, to be still for specific seconds and to repeat the cycle the desired times. Then, the procedure takes place in a flawless and objective way, in order then to be correctly compared with other tests where the variables are different.

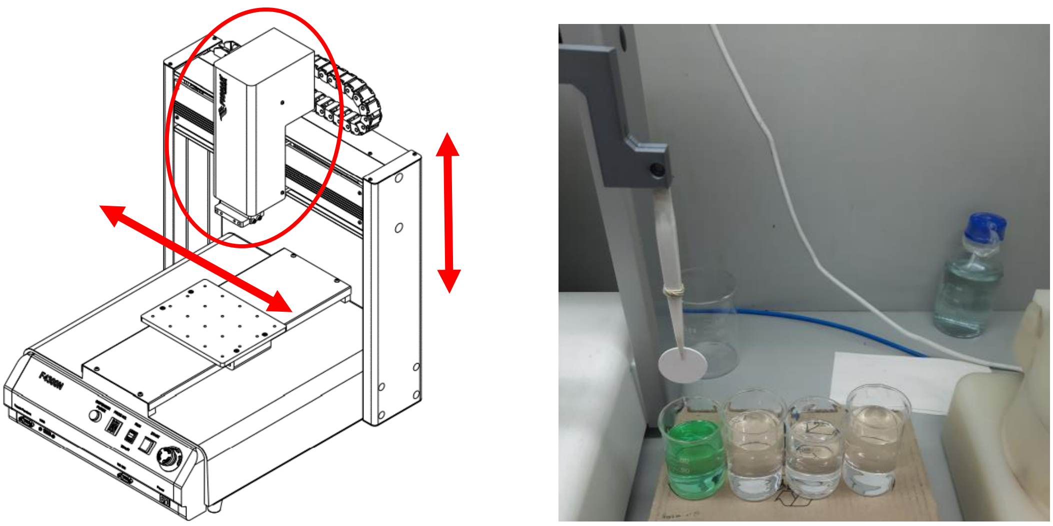

Figure 16: ROBOT- F4000N.1 SERIES, where the red arrows show the direction and sense of the movement (left); and image of SILAR experimental setup (right).

3.2.2.1 Experimental Procedure

The only cationic precursor used was 0.1 M $[Ni(H_2O)_2(NH_3)_4]^{2+}$. The solution is made by diluting nickel nitrate $Ni(NO_3)_2·6H_2O$ in ammonium hydroxide (NH_4OH) at room temperature; *i.e.* before the dilution of the solid $Ni(NO_3)_2·6H_2O$ in the deionized water, some drops of diluted NH_4OH were inserted in water until the pH reached 9, obtaining the complex nickel $[Ni(H_2O)_2(NH_3)_4]^{2+}$. This solution was maintained at room temperature (25 °C).

The two anionic precursors used were hydrogen peroxide (H_2O_2) and sodium hydroxide (NaOH). The H_2O_2 solution used was 1 % v/v, which was maintained at 85 °C, using a heating plate. The NaOH solutions used were 0.01 M and 0.1 M, at room temperature (25 °C). Contrarily to the SILAR procedure shown in the Figure 15 and to most of the literature where this procedure is utilized, when the anionic precursor utilized was H_2O_2 the rinse solution was excluded, as reported elsewhere [64]. When the anionic precursor utilized was NaOH, ultra-pure water was used as the rinse solution, between the two precursors. After the SILAR deposition, the catalytic membranes were calcinated. The oven, where the substrates were inserted, was set to raise 1 °C min^{-1}, from 20 °C to 600 °C (580 min) and stayed at this temperature for 5 h, before being cooled down to the room temperature (1 °C min^{-1}).

To study the amount of catalyst deposited and its morphology, there were changed certain variables between all the experiment, such as the concentration of the solutions, the number of cycles, the time of dipping and the calcination were altered throughout the tests. Due to the innumerous variables and membranes made, it was created a nomenclature system in order to identify the production variables by the name of the membrane. Each set of characters of the membrane name has a meaning and attended the following guidelines:

- The first letter – N or H – stands for the anionic precursor, NaOH or H_2O_2.
- The second part stand for the concentration of the previous anionic precursor: when it is H_2O_2 1 %(v/v) - 1. For the case of 0.01 M NaOH - 0; 0.1 M NaOH – 1.
- The third and final characters are related to the number of cycles done – 40, which means 40 cycles of dipping.

Examples of the application of the nomenclature method created are shown in Table 2.

Table 2: Examples of the Nomenclature for the Catalytic Membranes.

Membrane Name	*Cationic Precursor*	*Anionic Precursor*	*Anionic precursor Concentration*	*Number of cycles*
N1-40	$Ni(NO_3)_2$	NaOH	0.1 M	40
N0-30	$Ni(NO_3)_2$	NaOH	0.01 M	30
H1-20	$Ni(NO_3)_2$	H_2O_2	1 % (v/v)	20

3.3 Characterization of the Catalyst

3.3.1 Catalyst Tests

A planar membrane reactor designed and constructed within the scope of the European project 112CO2, from the collaborative work between LEPABE-UPORTO and Pixel Voltaic, was assembled with the as-prepared catalytic membranes to access their catalytic activity. The membranes are then placed between two end plates, using vermiculite gaskets to seal the substrate (horizontally), in a system like that of Solid Oxide Fuel Cells – Figure 17. The upper chamber consists in a nearly zero-gap between the substrate and the top plate. The catalytic layer faces downwards in the reactor, towards the lower chamber, which possesses a free volume, to allow free carbon growth without generating immediate clogging. Released carbon can be then accumulated at the bottom, far away from the catalytic layer. This reactor design is easy to assemble and disassemble, which is very important to perform several experiments needed to optimize the catalytic system and achieve its full regeneration multiple times.

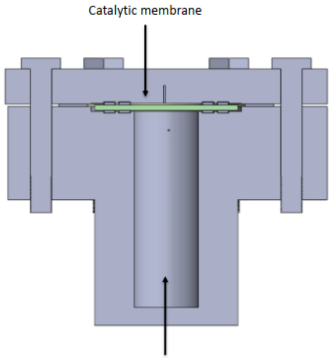

Figure 17: Planar membrane reactor- 112CO2 – Pixel Voltaic – LEPABE-UPORTO.

For the present work, the reactor was operated at 550 °C inside an oven, feeding 10 ml min^{-1} of methane, and operated for 60 min. The feed current is 100 cm^3 min^{-1}, made of 90 % N_2 and 10 % CH_4 (v/v). The catalytic performance was evaluated through both methane conversion (X_{CH4}) and hydrogen activity (a), assuming ideal gas behavior for all used gases at operation conditions, equations (8) and (9), respectively.

$$X_{\mathrm{CH4}} = \frac{x_{\mathrm{H2}}}{x_{\mathrm{H2}} + 2x_{\mathrm{CH4}}} \tag{8}$$

$$\alpha = \frac{\dot{m}_{\mathrm{H2}}}{W} = 60\frac{\rho_{\mathrm{H2}} x_{\mathrm{H2}} F_{\mathrm{out}}}{W} \tag{9}$$

Where a is hydrogen production activity in $g_{H2}\, g_{Ni}^{-1}\, h^{-1}$, $\dot{m}_{\mathrm{H2}}$ is hydrogen mass flowrate in $g_{H2}\, h^{-1}$, W is catalyst (Ni phase) mass in g_{Ni}, ρ_{H2} is hydrogen density at normal pressure and temperature (NPT) conditions in $g_{H2}\, ml^{-1}$, x_{H2} is hydrogen molar (volumetric) fraction, F_{out} is the reactor outlet volume flow at NPT conditions in ml·min^{-1}, X_{CH4} is methane conversion and x_{CH4} is methane molar (volumetric) fraction.

3.3.2 Scanning Electron Microscopy (SEM)

The morphology of the surface of the membrane is a key characteristic to understand the performance differences obtained. The scanning electron microscope is one of the most versatile equipment for examining and analyzing the morphology of microstructures and their chemical composition. The microscope used was a Phenom XL Desktop available at LEPABE (Figure 18), and the SEM images were processed using ProSuite Software. The acceleration voltage was 15 keV while an in-lens detector was employed with a working distance of 10 mm.

The specimen's different signals can be gathered and utilized to create pictures, and two different imaging method were used: Secondary Electron Display (SED) - are those electrons that depart the sample with energies below 50 eV and are typically expelled from their orbits around an atom by an incoming electron. They primarily provide topography data, but some compositional contrast is also visible. Backscattered Electron Display (BSD) - Backscattered electrons are incident electrons that come close enough to an atom's nucleus to scatter widely and reappear from the surface. The majority of the time, they reveal compositional information, brighter contrast is produced by components with higher atomic masses [66].

3.3.3 Inductively Coupled Plasma Mass Spectrometry (ICP-MS)

In order to know the exact amount of catalyst that was deposited in the substrate, after the SILAR procedure, the membrane was submitted to Inductively Coupled Plasma Mass Spectrometry (ICP-MS). It is important to refer that the amount of Ni deposited is in the order of magnitude of micrograms, so a normal balance is not capable of a precise measurement. Using the ICP-MS technique (Figure 19; Thermo Fisher, model iCAP™ 7400 ICP-OES Analyzer), it is possible to get exact values. The membrane is first subjected to a digestion process in a solution of Aqua Regia (a mixture of nitric and hydrochloric acid, in a molar ratio of 1:3, highly corrosive), where all the NiO deposited is extracted. Finally, the membrane is removed, and the solution is diluted into a known volume and the mass of NiO is measured.

Figure 18: SEM - Phenom XL Desktop.

Figure 19: iCAP™ 7400 ICP-OES Analyzer.

4 Results and Discussion

For the anionic precursors, H_2O_2 and NaOH were used as a weak and a strong precursor, respectively. As explained before, repeated immersion of the substrate into the solutions cause further growth of nucleation sites and it forms clusters or a film on the substrate. After a certain number of deposition cycles, the substrate will still attract Ni^{2+}, but as the thickness of $Ni(OH)_2$ increases, the attraction force decreases as nucleation sites become saturate, which leads to the decrease of the deposition rate. In the calcination step, this hydroxide phase is converted into an oxide phase by the calcination at 600 °C (eq.10), to form the NiO film. The calcination temperature occurs at 600 °C, 50 °C higher than the reaction temperature.[64]

$$2\mathrm{Ni(OH)_2} \rightarrow 2\mathrm{NiO} + \mathrm{H_2O} \tag{10}$$

4.1 H_2O_2 as the Anionic Precursor

4.1.1 H_2O_2 1 % v/v

As a starting point, an experimental setup was assembled for performing the SILAR depositions; the procedure was adapted from the work reported by Das *et al.*[64] The authors stated that a substrate subjected to 40 cycles showed the best morphologic characteristics, namely grain size, porosity, *etc*. Therefore, the first catalytic membrane was performed with a H_2O_2 solution of 1 % v/v as the anionic precursor and the SILAR procedure was repeated for 40 cycles; this sample is hereafter called as H1-40. Table 3 summarizes the conditions used for the production of the membrane H1-40.

Table 3: H_2O_2 Membrane – SILAR Procedure.

Membrane	Cationic Precursor	Anionic Precursor	Anionic precursor Volume Fraction	Number of cycles
H1-40	$Ni(NO_3)_2$	H_2O_2	1 %	40

From SEM analysis, it is noticeable that the H1-40 membrane presented a low deposition and poor dispersion. This phenomenon is clear in Figure 20, where there is a zone, the upper half, presenting substantial aggregations of NiO (white particles), and a large area where the catalyst was not deposited, bottom half.

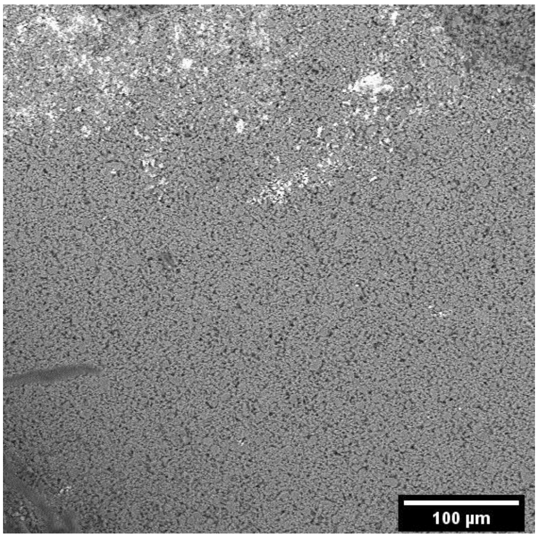

Figure 20: H1-40 – SEM image (BSD) - Top View - 320x.

Figure 21 shows a zoom-in of Figure 20 (deposition zone), where particle size ranges from *ca*. 50 nm to 10 µm. It is clear that Ni particles tend, along the SILAR cycles, to deposit onto the as-deposited Nickel areas, *i.e.* have preferential areas; this allows forming NiO agglomerates and not a uniform deposition as expected. The method used to measure the particles has its limits and the smaller particles sizes could not be precisely determined in the maximum zoom-in, as well as the large particles correspond to the large agglomerates of small particles that were arduous to distinguish; for those reasons, a particle size histogram was not performed in this case.

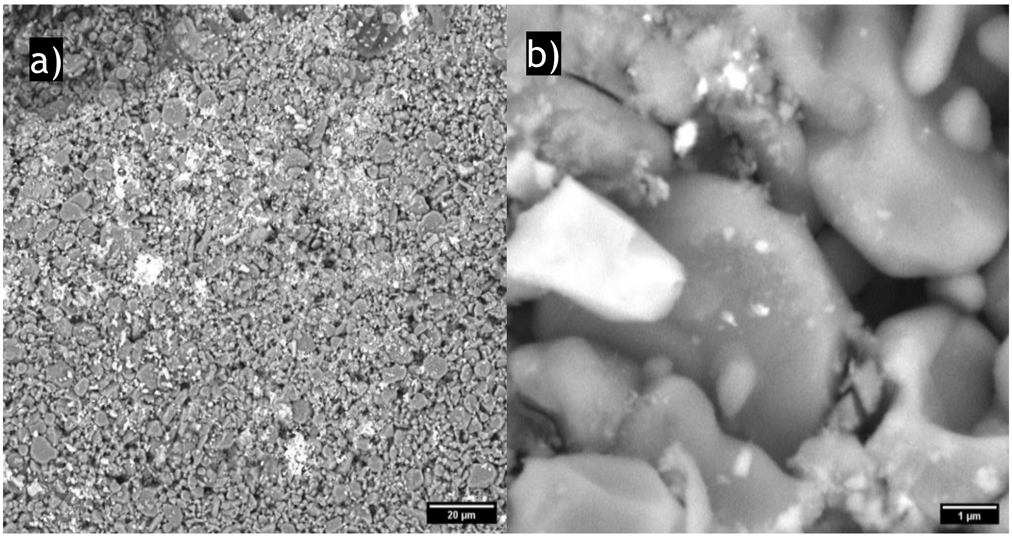

Figure 21: H1-40 – SEM images (BSD) - Top View - a) 1700x b) 28500x.

Catalytic performance was evaluated through both hydrogen activity and methane conversion, assuming ideal gas behavior for all used gases at operation conditions, as explained before. Figure 22 shows the methane conversion, X_{CH4}, and hydrogen activity, *a,* measured during one cycle of 1 h and Table 4 summarizes all the results obtained for the catalyst H1-40.

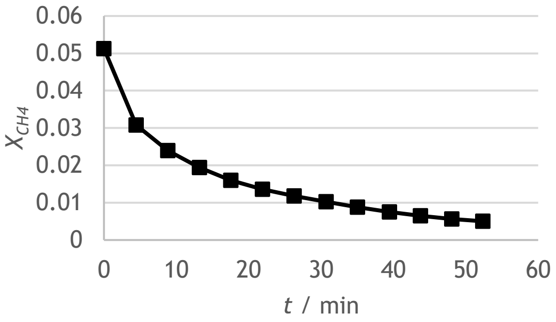

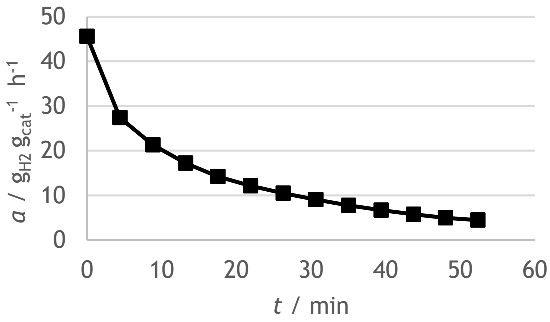

Figure 22: Hydrogen production activity from catalytic methane decomposition obtained for membrane H1-40: conversion and activity over decomposition time.

The H1-40 membrane reached a maximum hydrogen activity of *ca.* 45.6 $g_{H2}\ g_{cat}^{-1}\ h^{-1}$, with an average of *ca.* 14.4 $g_{H2}\ g_{cat}^{-1}\ h^{-1}$ during 1 h. To the best knowledge of the authors, the obtained activities are 8.5 and 3 times higher than the best catalyst ever reported, respectively for the peak and average activities. These results in comparison with the literature (Table 1) are remarkable, despite the low amount of NiO catalyst deposited (0.112 mg measured by ICP analysis) and its poor dispersion (shown by SEM images). Moreover, it was verified that both conversion and activity tend to decrease over decomposition time. This is due to the carbon deactivation in the active sites of the catalyst. It seems that these active sites, although having the ideal characteristics, are prone to tip-growth mechanism that detaches Ni particles reducing the catalytic surface area [67]. Concerning the methane conversion, it was also observed an initial peak of *ca.* 5.1 % and an average conversion of *ca.* 1.6 %, but these values are lower than the ones reported in literature. The conversion is related to the methane feed and the resulting hydrogen produced, which means that the feed is much higher than what will be after further optimization. If the feed flow is reduced or if the catalyst loading inside the area of reactor is higher, the conversion will be closer to the equilibrium conversion. However, in order to maintain the same conditions for all the membranes, these parameters were not changed.

Although the unprecedented results presented in Table 4, the deposition of NiO was not uniform over the substrate, as observed from the SEM analysis (Figure 20). This is of major importance for long-term tests and for enhancing the hydrogen production. Therefore, the parameters of the SILAR procedure had to be changed, *i.e.* the number of cycles or the time of dipping in each precursor, as well as the anionic precursor to NaOH.

Table 4: H1-40 Membrane - Performance Evaluation.

Membrane	Mass of Catalyst (mg)	Peak Conversion	Average Conversion	Peak Activity ($g_{H2}\ g_{cat}^{-1}\ h^{-1}$)	Average Activity ($g_{H2}\ g_{cat}^{-1}\ h^{-1}$)
H1-40	0.122	0.0513	0.0162	45.6	14.4

4.2 NaOH as the Anionic Precursor

4.2.1 0.1 M NaOH – Without Rinse

To understand the role of the anionic precursor in the membranes preparation, the other parameters of the SILAR procedure under study were maintained constant. Therefore, the NaOH concentration tested was 0.1 M, and the procedure followed was similar to when the precursor was H_2O_2, *i.e.* 3 dipping solutions (cationic, anionic and water), without rinse steps between the cationic and the anionic solution. For that reason, the name of this membrane has an additional "~" on top of the first letter (the initial N), meaning that, in this specific case, no rinse step was performed. Table 5 displays the parameters of the Ñ1-20 membrane prepared.

Table 5: Ñ1-20 – SILAR Procedure.

Membrane Name	Cationic Precursor	Anionic Precursor	Anionic precursor Concentration	Number of cycles
Ñ1-20	$Ni(NO_3)_2$	NaOH	0.1 M	20

The result was unforeseen, the Ñ1-20 membrane had a much higher deposition of NiO than H1-40. In Figure 23 is possible to observe that NiO particles detach from the substrate after removing the membrane from the calcination oven (600 °C), showing that the deposited catalyst suffered a delamination phenomenon. The amount of catalyst in the membrane was excessive and did not attached to the substrate when submitted to calcination, with the release of water vapor.

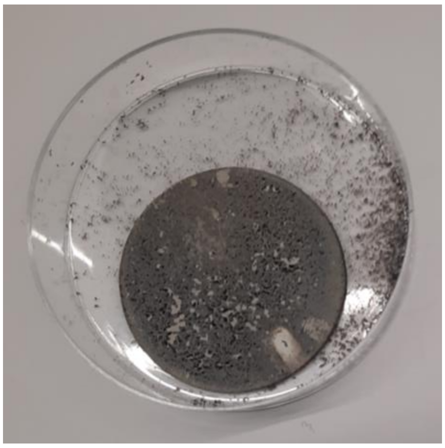

Figure 23: Ñ1-20 Membrane picture – Top View.

Figure 24a) shows that the particle size increased in comparison with H1-40 sample, showing a predominance of > 50 µm size particles. From the cross-section view - Figure 24b) it is possible to observe that, along the SILAR cycles of production, Ni also preferred to deposit on top of as-deposited Ni and not uniformly over the entire substrate surface. The particles formed a particular shape that detach from the substrate, corroborating what was visually observed. This may be justified to the absence of a rinse step in the synthesis of the membrane, which allowed the deposition of excessive Ni particles, since the deposition is faster and less controlled. Therefore, it contributed to a growth of nickel agglomerations made from unbounded ions and the substrate to be dipped in the following anionic precursor with more than only one ionic layer of Ni^{2+}. This occurrence happens when strong anionic precursors are utilized because, when inserted in the solution, almost all the Ni^{2+} particles will react with OH^- to form NiO. Once this phenomenon was observed, the membrane was not tested in the reactor. In order to avoid this type of results, and due to the difference in the strength of these two anionic precursors, it was added a rinse step between the cationic and the anionic precursor. Moreover, to reduce the time of deposition and obtain more uniform layers of catalyst, it was decreased the concentration of NaOH to 0.01 M, as described elsewhere [68], [69]. Therefore, the SILAR procedure followed the steps shown in Figure 15 scheme, with 4 dipping solutions.

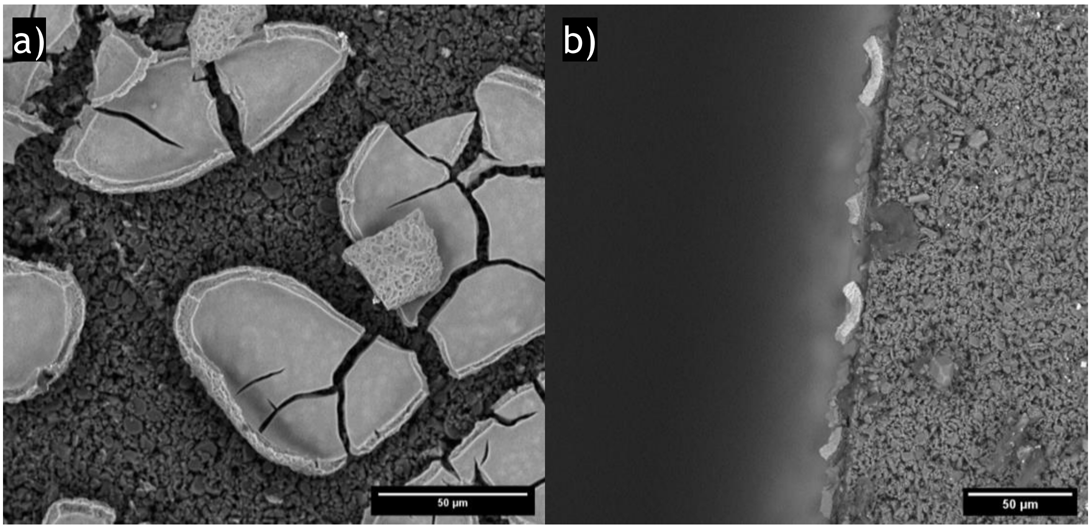

Figure 24: Ñ1-20 Membrane – SEM Images (BSD) - a) Top View - 1450x b) Cross Section – 860x.

4.2.2 0.01 M NaOH – Rinse

The SILAR procedures of production of the membranes utilizing 0.01 M NaOH are displayed in Table 6. From top view SEM images (Figure 25), the membranes (at different magnifications) showed a smooth deposition of Ni (white dots) over the entire substrate. It was observed that increasing the number of cycles clearly results in a better deposition, both in terms of particle size and dispersion of the nucleation sites, and that the catalyst tend to deposit not only on the surface of the substrate but also underneath.

Table 6: N0 – SILAR Procedure.

Membrane Name	Cationic Precursor	Anionic Precursor	Anionic precursor Concentration	Number of cycles
N0-20	$Ni(NO_3)_2$	NaOH	0.01 M	20
N0-40	$Ni(NO_3)_2$	NaOH	0.01 M	40

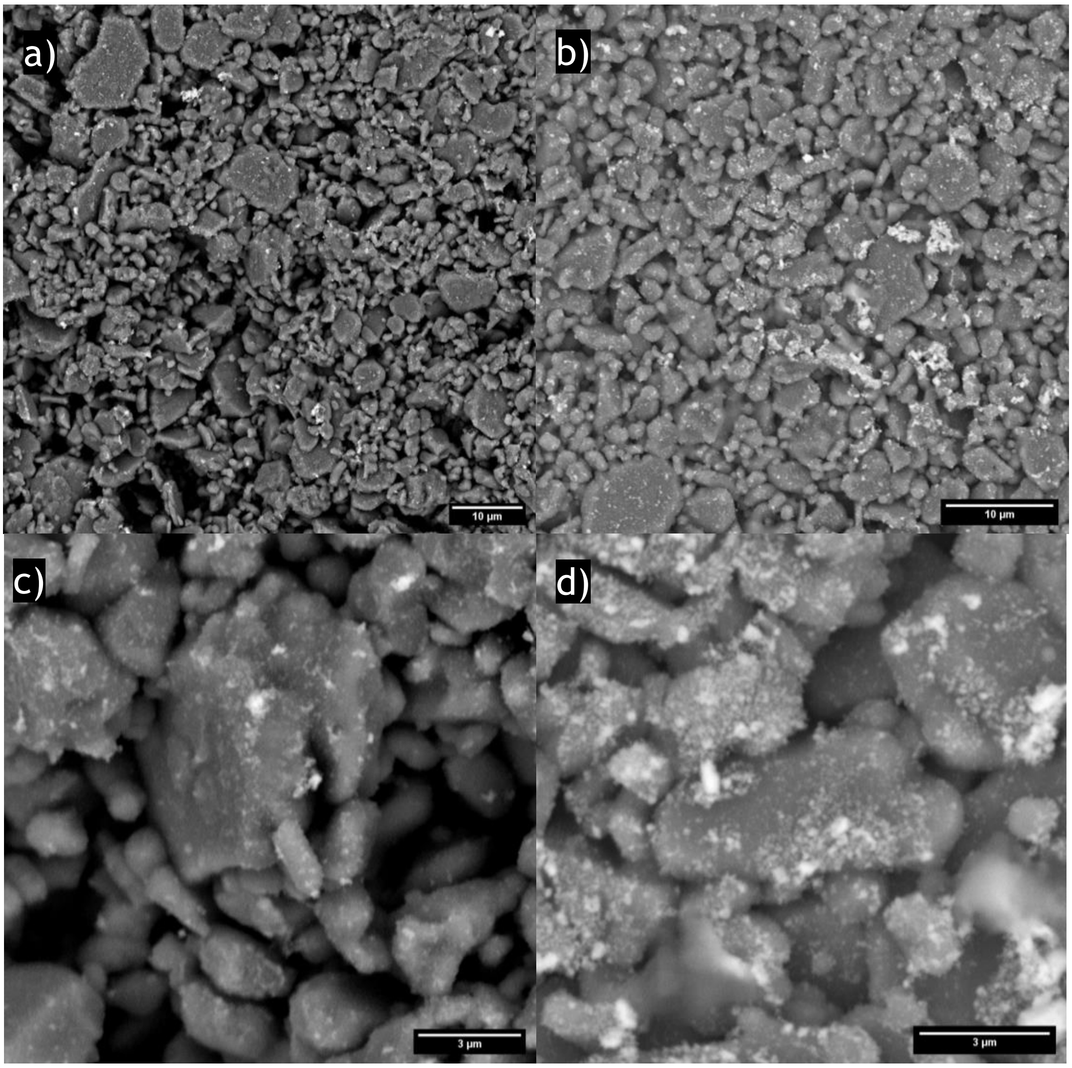

Figure 25: N0 - Top View – SEM images (BSD) - 4 000x – a) N0-20 b) N0-40 - 20 000x - c) N0-20 d) N0-40.

For both membranes, it was possible to measure the size of the Ni particles and analyze their frequency, as shown in the histogram plots (Figure 26). As previously mentioned, the membrane N0-40 (with 40 cycles) presented Ni particles with larger diameters, *i.e.* the frequency of particles size is in the range of 0.075 – 0.125 µm, whereas the Ni particles size for membrane N0-20 tends to vary mainly in the range of 0.050 – 0.100 µm. Concerning the mass of catalyst deposited determined by ICP, N0-20 and N0-40 presented 0.333 mg and 0.459 mg, respectively, which is almost 3 to 4 higher than the membrane prepared with H_2O_2 solution. Then, the membranes were placed in the reactor and the behavior of hydrogen activity, and methane conversion was evaluated during the decomposition time (1 h) - Figure 27.

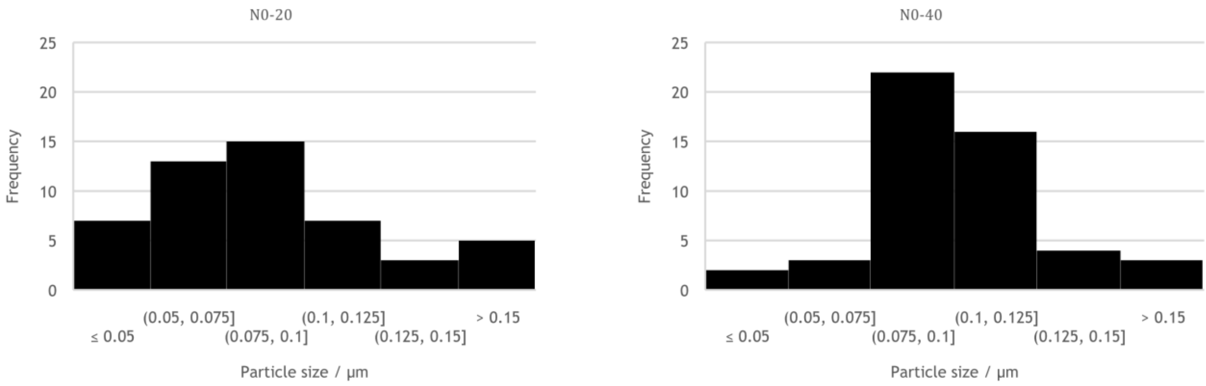

Figure 26: N0 – Particle Size Histograms.

The membranes were then placed in the reactor and their performance was evaluated over 1 h. Figure 27 shows the behavior of activity, *a*, and conversion, X_{CH4} along decomposition time. From ICP tests, the mass of the membranes N0-20 and N0-40 was 0.333 mg and 0.459 mg, respectively. The N0-20 membrane reached a methane conversion peak of *ca.* 5.3 % and an average conversion of *ca.* 2.1 %; in terms of the hydrogen activity, *ca.* 17.2 g_{H2} g_{cat}^{-1} h^{-1} was the activity peak and the average was *ca.* 6.70 g_{H2} g_{cat}^{-1} h^{-1}. For the N0-40 membrane, the conversion peaks with *ca.* 10.5 % and an average of *ca.* 4.6 %, while the activity peak was *ca.* 24.7 g_{H2} g_{cat}^{-1} h^{-1} and the average activity was *ca.* 10.9 g_{H2} g_{cat}^{-1} h^{-1}.

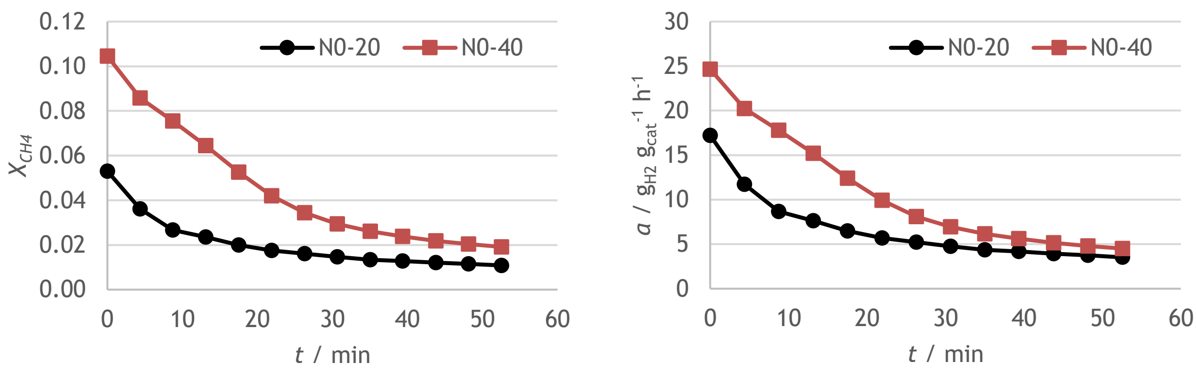

Figure 27: Hydrogen production activity from catalytic methane decomposition obtained for the NaOH - 0.01 membranes: conversion and activity over decomposition time.

The hydrogen activity and the methane conversion curves of the membranes N0-20 and N0-40 followed the similar trend shape observed with H1-40, i.e. these membranes reached the performance peak at the beginning and decreased along the decomposition time, suggesting that the active sites for the methane decomposition reaction are being covered by solid carbon, as previously expected. Table 7 summarizes the obtained performance results.

Table 7: N0 - Performance Evaluation.

Membrane	Mass of Catalyst (mg)	Peak Conversion	Average Conversion	Peak Activity (g_{H2} g_{cat}^{-1} h^{-1})	Average Activity (g_{H2} g_{cat}^{-1} h^{-1})
N0-20	0.333	0.0530	0.0206	17.2	6.70
N0-40	0.459	0.105	0.0462	24.7	10.9

It is clear that the membrane N0-40 is more active that of the membrane N0-20, due to the fact that the specific surface area of NiO increased, existing more active sites for the methane decomposition reaction to occur. Despite both membranes presented greater results than the ones reported in literature (Table 1), they are lower than the ones obtained with the H1-40 membrane. This may be related to the size of the Ni particles and, therefore, the carbon growth mechanism associated. The change in the precursor made the nucleation more effective, but the rinse solution washed part of the cationic precursor from the membrane, resulting in Ni particles with smaller diameters even presenting similar morphological characteristics than the membrane H1-40. In order to increase the NiO particle size and amount of catalyst deposited over the surface of the membrane, the concentration of NaOH was raised to 0.1 M. The rinse solution was maintained, because it washes the excess and unbound ions, promoting more homogenous structures.

4.2.3 0.1 M NaOH – Rinse

Three types of membranes were prepared using 0.01 M NaOH and varying the number of cycles among 5, 10 and 15 cycles – N1-5, N1-10 and N1-15 samples, the SILAR procedures for their preparation are displayed in Table 8.

Table 8: N1 – SILAR Procedure.

Membrane Name	Cationic Precursor	Anionic Precursor	Anionic precursor Concentration	Number of cycles
N1-5	$Ni(NO_3)_2$	NaOH	0.1 M	5
N1-10	$Ni(NO_3)_2$	NaOH	0.1 M	10
N1-15	$Ni(NO_3)_2$	NaOH	0.1 M	15

In the SEM images (low magnification) shown in Figure 28, it is possible to observe how the NiO particles are agglomerating as the number of SILAR cycles are increasing. It suggests that the quantity of catalyst aggregations is higher and less dispersed for N1-15 sample. With higher SEM magnification (Figure 29), the main differences between the three membranes are more explicit, as well as the three stages of deposition. N1-5 membrane presents the first phase, where the catalyst almost only deposits on the substrate. N1-10 membrane starts to show deposition not only on the substrate, but also onto the previously deposited catalyst. N1-15 membrane gathers the two previous stages, *i.e.* forms a film of catalyst due to the connection between the formed agglomerations. The mass of the membranes N1-5, N1-10, and N1-15, determined from ICP, was *ca.* 0.374 mg, 0.601 mg, and 0.780 mg, respectively.

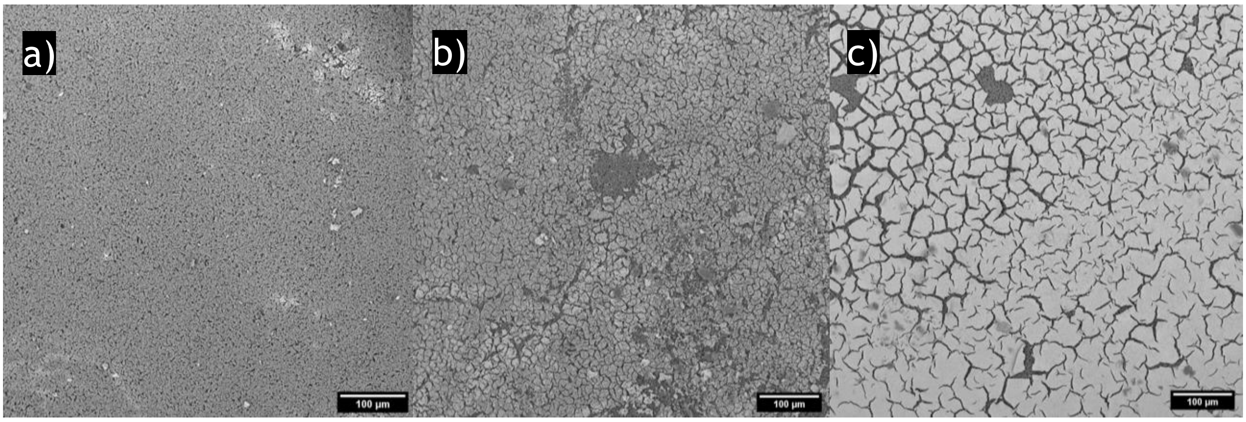

Figure 28: N1 - Top View – SEM Images (BSD) - 300x – a) N1-5 b) N1-10 c) N1-15.

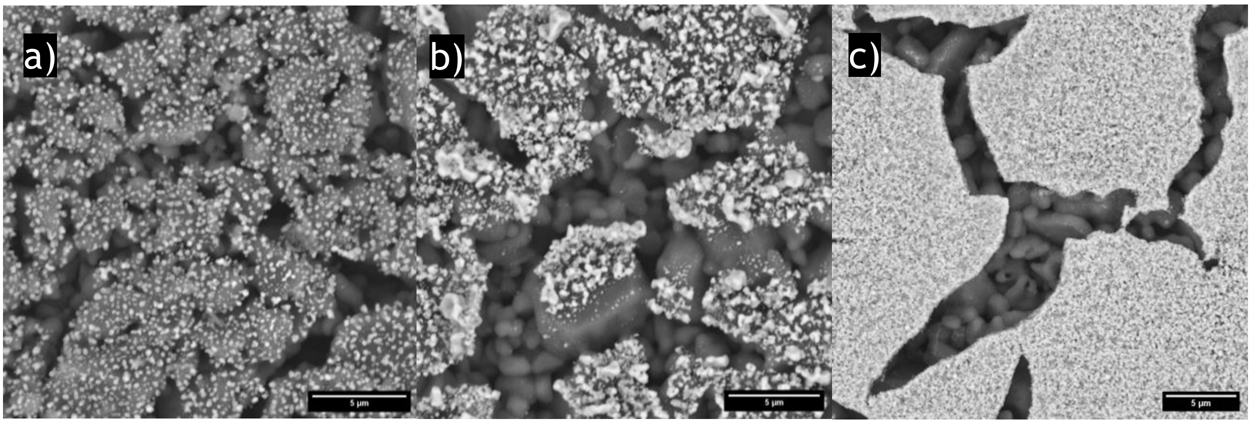

Figure 29: N1 - Top View – SEM Images (BSD) - 10 000x - a) N1-5 b) N1-10 c) N1-15.

From Figure 30 it was possible to draw the particle size histograms. The accumulation of Ni particles on already deposited catalyst in N1-10 membrane is easily verified, in comparison to N1-5, being the size of the clusters definitely increased. It exists a clear preference of Ni particles for attaching to itself instead of adsorbing in the surface of the substrate, which demonstrates the role of the first deposition cycles to form a more uniform and conformal film. The N1-15 membrane did not present differences regarding the previous pictures with lower magnification. Analyzing the histograms in Figure 31 and the SEM images, it is confirmed that the particle size increased with the increase of number of cycles. For the N1-5 membrane, the predominant particle size is between 0.2 μm and 0.3 μm, while for the N1-10 membrane it ranges from 0.350 - 0.475 μm. The analysis of the SEM images of N1-15 did not allow to measure the particle size and to construct the particles histogram, instead the formation of clusters, the catalyst formed a more compact film.

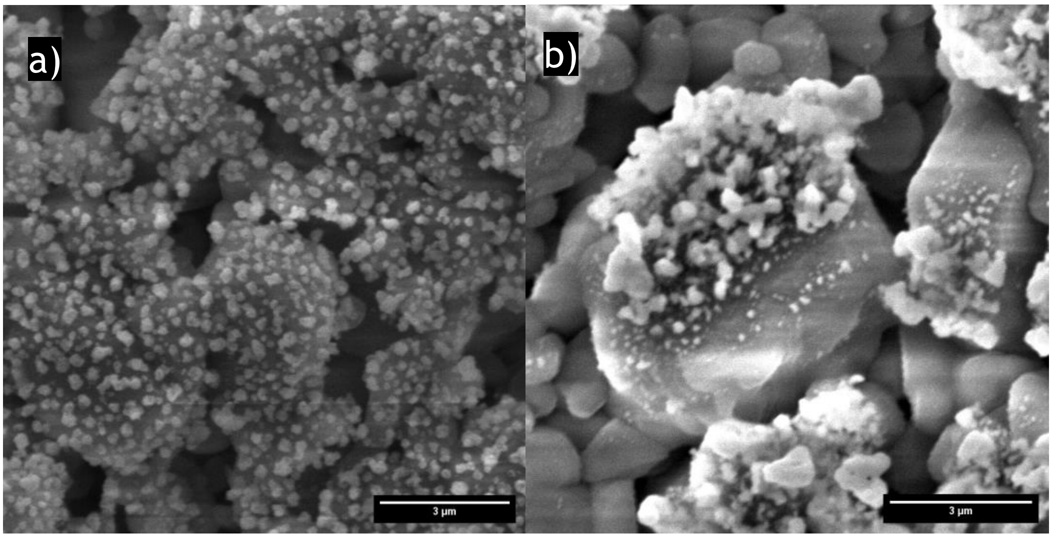

Figure 30: N1 - Top View - SED - 23 000x - a) N1-5 b) N1-10.

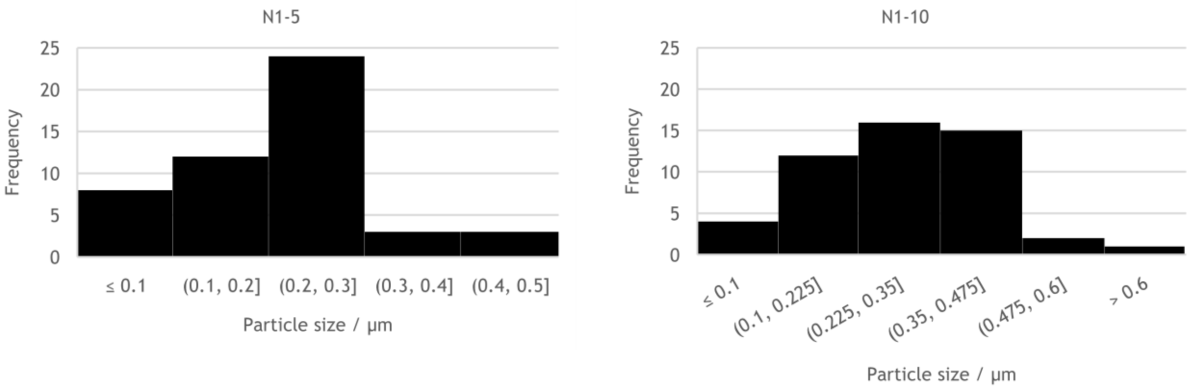

Figure 31: N1 - Particle Size Histograms.

Figure 32 displays the catalytic performance parameters obtained for these three membranes. The N1-5 membrane reached a conversion peak of *ca.* 4.2 % and an average value of *ca.* 1.6 %; the activity peak was *ca.* 12.1 g_{H2} g_{cat}^{-1} h^{-1} and the average activity was *ca.* 4.7 g_{H2} g_{cat}^{-1} h^{-1}. The N1-10 membrane shown a peak conversion of *ca.* 17.1 % and an average conversion of 12.9 %, while the peak activity was *ca.* 30.9 g_{H2} g_{cat}^{-1} h^{-1} and the average activity was 23.3 g_{H2} g_{cat}^{-1} h^{-1}. Finally, the N1-15 membrane shown a conversion peak of *ca.* 17.9 % and an average conversion of *ca.* 16.1 %; the peak activity was *ca.* 24.9 g_{H2} g_{cat}^{-1} h^{-1} and the average activity was *ca.* 22.3 g_{H2} g_{cat}^{-1} h^{-1}.

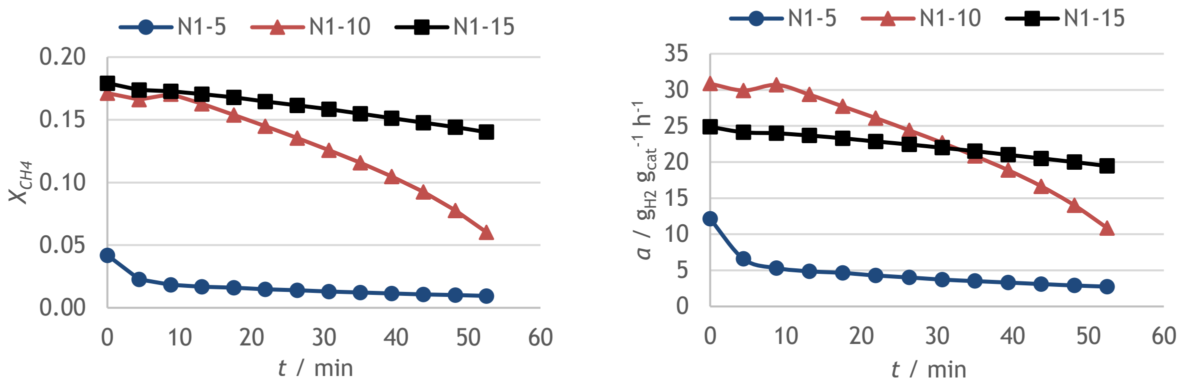

Figure 32: Hydrogen production activity from catalytic methane decomposition obtained for the NaOH - 0.1 membranes: activity and conversion over decomposition time.

The membrane that presents the higher methane conversion over the decomposition time was the one with the higher mass - N1-15. However, a different behavior was observer for the hydrogen activity, *i.e.* for the first 20 - 30 min the membrane showing the higher activities was N1-10, while membrane N1-15 was pretty stable over 1 h testing. Deactivation by the solid carbon produced is still the cause of this tendency; as expected, the membranes with lower amounts of catalysts deactivate faster owing to the fewer active sites. The conversion was expected to increase with the mass, since all the performance evaluation were operated with the same feed flow (10 mL min^{-1}), since more active sites will be available and, consequently, the reaction will be more complete. In opposition, the activity also depends on the specific surface area. Therefore, between the 10 and 15 cycles, with 0.1 M NaOH, it exists a maximum where the increase of mass no longer benefits the increase of surface area.

In summary, the N1-10 and N1-15 results are very impressive, the hydrogen activity peaks are 5.8 times and 4.7 times, respectively, higher than the best value in the literature (5.33 g_{H2} g_{cat}^{-1} h^{-1} - Table 1); the average activity is also higher (4.5 times and 4.2 times, respectively). The rising low values of conversion follow the justification stated for the previous membranes, as the catalyst mass increases, the methane conversion also raises (more reagent reacts).The performance of N1 membranes is summarized in Table 9.

Table 9: N1 - Performance Evaluation.

Membrane	Mass of Catalyst (mg)	Peak Conversion	Average Conversion	Peak Activity (g_{H2} g_{cat}^{-1} h^{-1})	Average Activity (g_{H2} g_{cat}^{-1} h^{-1})
N1-5	0.374	0.0420	0.0163	12.1	4.70
N1-10	0.601	0.171	0.129	30.9	23.3
N1-15	0.780	0.179	0.161	24.9	22.3

5 Conclusion

The low-temperature catalytic methane decomposition (CMD; typically 500 – 650 ºC) is an extraordinary process for continuously producing inexpensive and COx-free hydrogen and solid carbon. Currently at TRL 3-4, the industrialization of this technology has been hindered so far by the extremely fast catalyst deactivation, which is caused by the inevitable coverage of catalytic sites by the formed solid carbon. Therefore, the success of CMD depends on the development of an earth-abundant catalyst that is very active, stable, and regenerable, as well as on the design of the reactor. Both optimizations are of major interest for Pixel Voltaic that aims to industrialize this technology and for UPORTO-LEPABE that is leading the European project 112CO2 within the field.

The present work aimed at depositing a Ni-based catalytic membrane, without a separative function, to be integrated in a membrane reactor running at 550 ºC; NiO catalysts showed the highest activity and stability for CMD. Successive Ionic Layer Adsorption and Reaction (SILAR) was the technique used to deposit 2D thin and conformal films of NiO over Al_2O_3 ceramic substrates, which was never reported for these applications. SILAR is a simple and reproducible method, and it is easily scalable. The conditions of the SILAR deposition, such as the number of SILAR cycles, the precursors used and rising steps, were varied to study their role on the film morphology and catalytic activity. An experimental and automatic setup was assemble able to perform the SILAR deposition. First, the effect of the anionic precursor (H_2O_2 and NaOH) was analyzed, using $Ni(NO_3)_2{\cdot}6H_2O$ as the cationic precursor and with 40 SILAR cycles. Unprecedented catalytic results were obtained with catalytic membranes prepared using H_2O_2, *i.e.* it was achieved a hydrogen activity peak of *ca.* 45.6 $g_{H2}\ g_{cat}^{-1}\ h^{-1}$. However, the NiO deposition was not uniform over the entire substrate surface, as observed from SEM analysis, and the catalyst started to deactivate. This phenomenon was improved using 0.1 M NaOH as the anionic precursor, 10 SILAR cycles and rinse steps. The best-performing catalytic membrane showed an average catalytic activity of *ca.* 23.3 $g_{H2}\ g_{cat}^{-1}\ h^{-1}$ for 1 h, which is 3-4 times higher than the highest reported in the literature. The frequency of the particles size ranges from 0.350 μm to 0.475 μm and a mass of *ca.* 0.601 mg was determined by ICP.

The main conclusions to withdraw from the SILAR optimization study were: i) the raise in the number of cycles results in a larger particle size, as the Ni particles tend to deposit on top of the as-deposited catalyst; ii) the stability of the catalyst depends mainly on the amount of catalyst deposited over the entire surface. The greater is the catalyst weight, the longer the catalytic membrane maintains its initial (peak) activity, since the solid carbon by-product is going to deposit on the active sites of the catalyst, encapsulating and preventing the reagents to reach them and react; iii) each anionic precursor forms different structured agglomerations of NiO, H_2O_2 improved the morphology of the film allowing to achieve better hydrogen activities, whereas NaOH allowed to deposit more uniform layers that enhances the reaction stability.

6 Assessment of the Work Done

6.1 Objectives Achieved

The energy decarbonization is an urgent matter that humanity is facing nowadays. Disruptive and competitive energy technologies are needed to face the fast climate change and avoid its devastating consequences. Hydrogen has emerged as a clean, inexpensive and high energy density vector and the current technologies for its production were overviewed. In this work, the low-temperature catalytic methane decomposition (CMD) was the technology under study for producing clean hydrogen, which is expected to be better than the available described in the literature or disclosed by any company. Pixel Voltaic and LEPABE aimed to prepare Ni-based catalytic membranes based on 2D thin and conformal films to enhance catalytic activity and avoid the catalyst deactivation, caused by solid carbon formation. SILAR technique was used for the first time for this application and a setup bench-top was constructed to allow an automatic control using a programmable robot. The catalysts prepared showed record catalytic activities for hydrogen production when compared to literature, which encourages further optimizations.

6.2 Other Work Carried Out

Aside from the results presented, the regeneration capability of the prepared catalyst was also studied, performing long-term decomposition tests. In-depth characterization of the materials resulting from such experiments provided insights on the role of the ceramic support on carbon nucleation and anchoring of tip-growth mechanism. The understanding of these phenomena is of paramount importance to control the carbon behavior in the metal surface and subsurface, allowing tuning of the catalysts towards more stable and regenerable operation. It was implemented a cycle system, where the membrane would be subjected to a regeneration period followed by another production stage. Being a highly complex and time-consuming process, these tests were only performed for the most promising materials. Moreover, it is important to refer that a patent will be filled by Pixel Voltaic and UPORTO on the role of 2D catalytic membranes for CMD.

6.3 Limitations and future work

Due to the time available for the completion of this work, it was not able to perform a design of experiments (DoE) approach to optimize the catalytic activity of the membranes prepared, as expected. This tool would allow to study the influence of several parameters of the SILAR procedure and to understand their correlation with the morphological properties of the film. Moreover, there was a stock rupture for the used Ni precursor for almost two months, which limited the number of depositions performed. As future work, other SILAR variables can be studied, *e.g.* the cationic precursor, the time of dipping, the final rinse, the temperature of the precursor solution, *etc.* The role of the substrate pre-treatment proved to be inconclusive, but it will be the subject of study for obtaining better catalyst deposition and loading control.

6.4 Final Assessment

Throughout the course of this work, I was able of get insight regarding my professional expectations and ambitions. This experience has also provided me with a wealth of knowledge about professional life, learning working methodologies, and team cooperation. Additionally, this project gave me the opportunity to develop a strong interest and hope for the renewable energy sources, the hydrogen economy and specially the relevance of catalytic methane decomposition for producing clean hydrogen.

7 References

[1] IPCC-SAR, "Climate Change 1995: A report of the Intergovernmental Panel on Climate Change," 1995. [Online]. Accessed in March 2022. Available: https://archive.ipcc.ch/pdf/climate-changes-1995/ipcc-2nd-assessment/2nd-assessment-en.pdf%0Ahttps://www.ipcc.ch/site/assets/uploads/2018/05/2nd-assessment-en-1.pdf.

[2] C.-F. Schleussner *et al.*, "Science and policy characteristics of the Paris Agreement temperature goal," *Nat. Clim. Chang.*, vol. 6, no. 9, pp. 827–835, Sep. 2016, doi: 10.1038/nclimate3096.

[3] "Global Temperature Record," *The 2 Degrees Institute*, 2022. Accessed in March 2022. https://www.temperaturerecord.org/.

[4] "Global primary energy consumption by source," *Global and National Perspectives. & BP Statistical Review of World Energy.*, 2020. Accessed in March 2022. https://ourworldindata.org/energy-mix.

[5] N. Antonakakis, I. Chatziantoniou, and G. Filis, "Energy consumption, CO2 emissions, and economic growth: An ethical dilemma," *Renew. Sustain. Energy Rev.*, vol. 68, no. October 2015, pp. 808–824, 2017, doi: 10.1016/j.rser.2016.09.105.

[6] R. A. Hefner, "The age of energy gases," *Int. J. Hydrogen Energy*, vol. 27, no. 1, pp. 1–9, 2002, doi: 10.1016/S0360-3199(01)00079-9.

[7] D. Sadler *et al.*, "H21 Leeds City Gate Report," 2016. [Online]. Accessed in March 2022. Available:https://www.northerngasnetworks.co.uk/wp-content/uploads/2017/04/H21-Report-Interactive-PDF-July-2016.compressed.pdf.

[8] M. Wietschel and M. Ball, *The hydrogen economy: Opportunities and challenges*, vol. 9780521882. Cambridge: Cambridge University Press, 2009.

[9] P. E. Dodds and W. McDowall, "The future of the UK gas network," *Energy Policy*, vol. 60, pp. 305–316, 2013, doi: 10.1016/j.enpol.2013.05.030.

[10] U.S. Department of Energy, "H2@Scale," 2017. Accessed in March 2022. https://www.energy.gov/eere/fuelcells/h2scale.

[11] Essential Chemical Industry, "Hydrogen," 2016. Accessed in March 2022. https://www.essentialchemicalindustry.org/chemicals/hydrogen.html.

[12] A. E. Awadallah, M. S. Mostafa, A. A. Aboul-Enein, and S. A. Hanafi, "Hydrogen production via methane decomposition over Al2O 3-TiO2 binary oxides supported Ni

catalysts: Effect of Ti content on the catalytic efficiency," *Fuel*, vol. 129, pp. 68–77, 2014, doi: 10.1016/j.fuel.2014.03.047.

[13] International Energy Agency, "Transport, Energy and CO2: Moving toward Sustainability," 2009. Accessed in March 2022. https://www.iea.org/news/transport-energy-and-co2-moving-toward-sustainability.

[14] C. F. C. Partnership, "Air Climate, Energy, water Security: a guide to understanding the well-to-wheels impact of fuel cell electric vehicles."

[15] N. P. Brandon and Z. Kurban, "Clean energy and the hydrogen economy," *Philos. Trans. R. Soc. A Math. Phys. Eng. Sci.*, vol. 375, no. 2098, 2017, doi: 10.1098/rsta.2016.0400.

[16] J. Skea, "Research and evidence needs for decarbonisation in the built environment: A UK case study," *Build. Res. Inf.*, vol. 40, no. 4, pp. 432–445, 2012, doi: 10.1080/09613218.2012.670395.

[17] "112CO2." Accessed in March 2022. https://www.112co2.eu/.

[18] M. Steinberg, "Fossil fuel decarbonization technology for mitigating global warming," *Int. J. Hydrogen Energy*, vol. 24, no. 8, pp. 771–777, 1999, doi: 10.1016/S0360-3199(98)00128-1.

[19] M. Carmo, D. L. Fritz, J. Mergel, and D. Stolten, "A comprehensive review on PEM water electrolysis," *Int. J. Hydrogen Energy*, vol. 38, no. 12, pp. 4901–4934, Apr. 2013, doi: 10.1016/j.ijhydene.2013.01.151.

[20] K. E. Ayers *et al.*, "Research Advances towards Low Cost, High Efficiency PEM Electrolysis," *ECS Trans.*, vol. 33, no. 1, pp. 3–15, Oct. 2010, doi: 10.1149/1.3484496.

[21] X. Li, X. Hao, A. Abudula, and G. Guan, "Nanostructured catalysts for electrochemical water splitting: Current state and prospects," *J. Mater. Chem. A*, vol. 4, no. 31, pp. 11973–12000, 2016, doi: 10.1039/c6ta02334g.

[22] C. Hussy, "Water electrolysis explained – the basis for most Power-to-X processes," *Power-to-x*. Accessed in March 2022. https://ptx-hub.org/water-electrolysis-explained/.

[23] L. Alves, V. Pereira, T. Lagarteira, and A. Mendes, "Catalytic methane decomposition to boost the energy transition: Scientific and technological advancements," *Renew. Sustain. Energy Rev.*, vol. 137, no. September, 2021, doi: 10.1016/j.rser.2020.110465.

[24] S. Ardo *et al.*, "Pathways to electrochemical solar-hydrogen technologies," *Energy Environ. Sci.*, vol. 11, no. 10, pp. 2768–2783, 2018, doi: 10.1039/C7EE03639F.

[25] U. P. M. Ashik, W. M. A. Wan Daud, and J. ichiro Hayashi, "A review on methane

transformation to hydrogen and nanocarbon: Relevance of catalyst characteristics and experimental parameters on yield," *Renew. Sustain. Energy Rev.*, vol. 76, no. January, pp. 743–767, 2017, doi: 10.1016/j.rser.2017.03.088.

[26] B. J. Leal Pérez, J. A. Medrano Jiménez, R. Bhardwaj, E. Goetheer, M. van Sint Annaland, and F. Gallucci, "Methane pyrolysis in a molten gallium bubble column reactor for sustainable hydrogen production: Proof of concept & techno-economic assessment," *Int. J. Hydrogen Energy*, vol. 46, no. 7, pp. 4917–4935, Jan. 2021, doi: 10.1016/j.ijhydene.2020.11.079.

[27] W. E. Slater, "XV.—The influence of different surfaces on the decomposition of methane," *J. Chem. Soc., Trans.*, vol. 109, no. 160, pp. 160–164, 1916, doi: 10.1039/CT9160900160.

[28] N. Muradov, "Hydrogen via methane decomposition: An application for decarbonization of fossil fuels," *Int. J. Hydrogen Energy*, vol. 26, no. 11, pp. 1165–1175, 2001, doi: 10.1016/S0360-3199(01)00073-8.

[29] International Organization for Standardization, "ISO 14687 - Hydrogen fuel quality — Product specification," 2019, p. 17.

[30] N. S. N. Hasnan, S. N. Timmiati, K. L. Lim, Z. Yaakob, N. H. N. Kamaruddin, and L. P. Teh, "Recent developments in methane decomposition over heterogeneous catalysts: an overview," *Mater. Renew. Sustain. Energy*, vol. 9, no. 2, pp. 1–18, 2020, doi: 10.1007/s40243-020-00167-5.

[31] G. Wang, Y. Jin, G. Liu, and Y. Li, "Production of Hydrogen and Nanocarbon from Catalytic Decomposition of Methane over a Ni-Fe/Al 2 O 3 Catalyst," *Energy & Fuels*, vol. 27, no. 8, pp. 4448–4456, Aug. 2013, doi: 10.1021/ef3019707.

[32] P. Wang *et al.*, "Filamentous carbon prepared by the catalytic pyrolysis of CH4 on Ni/SiO2," *Appl. Catal. A Gen.*, vol. 231, no. 1–2, pp. 35–44, May 2002, doi: 10.1016/S0926-860X(01)00906-1.

[33] Y. Shen and A. C. Lua, "Synthesis of Ni and Ni–Cu supported on carbon nanotubes for hydrogen and carbon production by catalytic decomposition of methane," *Appl. Catal. B Environ.*, vol. 164, pp. 61–69, Mar. 2015, doi: 10.1016/j.apcatb.2014.08.038.

[34] J. Ashok, G. Raju, P. S. Reddy, M. Subrahmanyam, and A. Venugopal, "Catalytic decomposition of CH4 over NiO–Al2O3–SiO2 catalysts: Influence of catalyst preparation conditions on the production of H2," *Int. J. Hydrogen Energy*, vol. 33, no. 18, pp. 4809–4818, Sep. 2008, doi: 10.1016/j.ijhydene.2008.06.004.

[35] S. Takenaka, S. Kobayashi, H. Ogihara, and K. Otsuka, "Ni/SiO2 catalyst effective for

methane decomposition into hydrogen and carbon nanofiber," *J. Catal.*, vol. 217, no. 1, pp. 79–87, 2003, doi: 10.1016/S0021-9517(02)00185-9.

[36] S. Takenaka, H. Ogihara, I. Yamanaka, and K. Otsuka, "Decomposition of methane over supported-Ni catalysts: effects of the supports on the catalytic lifetime," *Appl. Catal. A Gen.*, vol. 217, no. 1–2, pp. 101–110, Sep. 2001, doi: 10.1016/S0926-860X(01)00593-2.

[37] N. D. Charisiou *et al.*, "An in depth investigation of deactivation through carbon formation during the biogas dry reforming reaction for Ni supported on modified with CeO2 and La2O3 zirconia catalysts," *Int. J. Hydrogen Energy*, vol. 43, no. 41, pp. 18955–18976, 2018, doi: 10.1016/j.ijhydene.2018.08.074.

[38] M. Kumar and Y. Ando, "Chemical vapor deposition of carbon nanotubes: A review on growth mechanism and mass production," *J. Nanosci. Nanotechnol.*, vol. 10, no. 6, pp. 3739–3758, 2010, doi: 10.1166/jnn.2010.2939.

[39] J. C. Guevara *et al.*, "Ni/Ce-MCM-41 mesostructured catalysts for simultaneous production of hydrogen and nanocarbon via methane decomposition," *Int. J. Hydrogen Energy*, vol. 35, no. 8, pp. 3509–3521, 2010, doi: 10.1016/j.ijhydene.2010.01.068.

[40] T. Zhang and M. D. Amiridis, "Hydrogen production via the direct cracking of methane over silica-supported nickel catalysts," *Appl. Catal. A Gen.*, vol. 167, no. 2, pp. 161–172, 1998, doi: 10.1016/S0926-860X(97)00143-9.

[41] N. D. Charisiou, S. L. Douvartzides, G. I. Siakavelas, L. Tzounis, K. Polychronopoulou, and M. A. Goula, "The Relationship between Reaction Temperature and Carbon Deposition on Nickel Catalysts Based on," *Catalysts*, vol. 9, no. 8, p. 676, 2019.

[42] E. R. Gilliland and P. Harriott, "Reactivity of Deposited Carbon," *Ind. Eng. Chem.*, vol. 46, no. 10, pp. 2195–2202, 1954, doi: 10.1021/ie50538a052.

[43] J. L. Figueiredo and D. L. Trimm, "Gasification of carbon deposits on nickel catalysts," *J. Catal.*, vol. 40, no. 2, pp. 154–159, 1975, doi: 10.1016/0021-9517(75)90241-9.

[44] J. X. Qian *et al.*, "Methane decomposition to produce COx-free hydrogen and nano-carbon over metal catalysts: A review," *Int. J. Hydrogen Energy*, vol. 45, no. 15, pp. 7981–8001, 2020, doi: 10.1016/j.ijhydene.2020.01.052.

[45] U. P. M. Ashik, W. M. A. Wan Daud, and H. F. Abbas, "Production of greenhouse gas free hydrogen by thermocatalytic decomposition of methane – A review," *Renew. Sustain. Energy Rev.*, vol. 44, pp. 221–256, Apr. 2015, doi: 10.1016/j.rser.2014.12.025.

[46] H. F. Abbas and W. M. A. Wan Daud, "Hydrogen production by methane decomposition: A review," *Int. J. Hydrogen Energy*, vol. 35, no. 3, pp. 1160–1190, 2010, doi: 10.1016/j.ijhydene.2009.11.036.

[47] P. Ammendola *et al.*, "Some issues in modelling methane catalytic decomposition in fluidized bed reactors," vol. 33, pp. 2679–2694, 2008, doi: 10.1016/j.ijhydene.2008.03.033.

[48] D. C. Upham *et al.*, "Catalytic molten metals for the direct conversion of methane to hydrogen and separable carbon," *Science (80-.).*, vol. 358, no. 6365, pp. 917–921, 2017, doi: 10.1126/science.aao5023.

[49] L. J. J. Catalan and E. Rezaei, "Coupled hydrodynamic and kinetic model of liquid metal bubble reactor for hydrogen production by noncatalytic thermal decomposition of methane," *Int. J. Hydrogen Energy*, vol. 45, no. 4, pp. 2486–2503, Jan. 2020, doi: 10.1016/j.ijhydene.2019.11.143.

[50] A. Bode *et al.*, "Methane Pyrolysis and CO 2 Activation - Technologies with Application Options for Hydrogen, Carbon and Synthesis Gas Production," *Chemie Ing. Tech.*, vol. 88, no. 9, pp. 1342–1342, Sep. 2016, doi: 10.1002/cite.201650483.

[51] BASF, "BASF Research Press Conference," 2019. Accessed in April 2022. https://www.basf.com/global/en/media/events/2019/basf-research-press-conference.html.

[52] C. Algieri *et al.*, "Catalytic membrane reactors: The industrial applications perspective," *Catalysts*, vol. 11, no. 6, 2021, doi: 10.3390/catal11060691.

[53] T. Westermann and T. Melin, "Flow-through catalytic membrane reactors-Principles and applications," *Chem. Eng. Process. Process Intensif.*, vol. 48, no. 1, pp. 17–28, 2009, doi: 10.1016/j.cep.2008.07.001.

[54] A. M. M. Mendes, C. Mateos Pedrero, and M. Dias Catarino, "WO2020121287 - Catalytic methane decomposition and catalyst regeneration, methods and uses thereof," PCT/IB2019/060868, 2020.

[55] Y. F. Nicolau, "Solution deposition of thin solid compound films by a successive ionic-layer adsorption and reaction process," *Appl. Surf. Sci.*, vol. 22–23, no. PART 2, pp. 1061–1074, 1985, doi: 10.1016/0378-5963(85)90241-7.

[56] H. M. Pathan and C. D. Lokhande, "Deposition of metal chalcogenide thin films by successive ionic layer adsorption and reaction (SILAR) method," *Bull. Mater. Sci.*, vol. 27, no. 2, pp. 85–111, Apr. 2004, doi: 10.1007/BF02708491.

[57] R. W. Johnson, A. Hultqvist, and S. F. Bent, "A brief review of atomic layer deposition: From fundamentals to applications," *Mater. Today*, vol. 17, no. 5, pp. 236–246, 2014, doi: 10.1016/j.mattod.2014.04.026.

[58] P. O. Brien and J. Mcaleese, "Bath deposition of ZnS and CdS," *J. Mater. Chem.*, vol. 8,

no. 11, pp. 2309–2314, 1998.

[59] K. Borgohain and J. Singh, "Quantum size effects in CuO nanoparticles," *Phys. Rev. B - Condens. Matter Mater. Phys.*, vol. 61, no. 16, pp. 11093–11096, 2000, doi: 10.1103/PhysRevB.61.11093.

[60] K. Mylvaganam, Y. Chen, W. Liu, M. Liu, and L. Zhang, "Hard thin films: Applications and challenges," *Anti-Abrasive Nanocoatings Curr. Futur. Appl.*, pp. 544–567, 2014, doi: 10.1016/B978-0-85709-211-3.00021-2.

[61] S. P. Ratnayake, J. Ren, E. Colusso, M. Guglielmi, A. Martucci, and E. Della Gaspera, "SILAR Deposition of Metal Oxide Nanostructured Films," *Small*, vol. 17, no. 49, 2021, doi: 10.1002/smll.202101666.

[62] B. O. Aronsson, J. Lausmaa, and B. Kasemo, "Glow discharge plasma treatment for surface cleaning and modification of metallic biomaterials," *J. Biomed. Mater. Res.*, vol. 35, no. 1, pp. 49–73, 1997, doi: 10.1002/(SICI)1097-4636(199704)35:1<49::AID-JBM6>3.0.CO;2-M.

[63] M. Lehocký and A. Mráček, "Improvement of dye adsorption on synthetic polyester fibers by low temperature plasma pre-treatment," *Czechoslov. J. Phys.*, vol. 56, no. SUPPL. 2, pp. 1277–1282, 2006, doi: 10.1007/s10582-006-0362-5.

[64] M. R. Das, A. Roy, S. Mpelane, A. Mukherjee, P. Mitra, and S. Das, "Influence of dipping cycle on SILAR synthesized NiO thin film for improved electrochemical performance," *Electrochim. Acta*, vol. 273, pp. 105–114, 2018, doi: 10.1016/j.electacta.2018.04.024.

[65] V. P. Tolstoy, "Successive ionic layer deposition. The use in nanotechnology," *Russ. Chem. Rev.*, vol. 75, no. 2, pp. 161–175, 2006, doi: 10.1070/rc2006v075n02abeh001197.

[66] K. D. Vernon-Parry, "Scanning electron microscopy: an introduction," *III-Vs Rev.*, vol. 13, no. 4, pp. 40–44, Jul. 2000, doi: 10.1016/S0961-1290(00)80006-X.

[67] Y. Li, D. Li, and G. Wang, "Methane decomposition to COx-free hydrogen and nano-carbon material on group 8-10 base metal catalysts: A review," *Catal. Today*, vol. 162, no. 1, pp. 1–48, 2011, doi: 10.1016/j.cattod.2010.12.042.

[68] U. M. Patil, K. V. Gurav, O. S. Joo, and C. D. Lokhande, "Synthesis of photosensitive nanograined TiO2 thin films by SILAR method," *J. Alloys Compd.*, vol. 478, no. 1–2, pp. 711–715, 2009, doi: 10.1016/j.jallcom.2008.11.160.

[69] A. U. Ubale, M. R. Belkhedkar, Y. S. Sakhare, A. Singh, C. Gurada, and D. C. Kothari, "Characterization of nanostructured Mn 3O 4 thin films grown by SILAR method at room temperature," *Mater. Chem. Phys.*, vol. 136, no. 2–3, pp. 1067–1072, 2012, doi: 10.1016/j.matchemphys.2012.08.052.